

Recent advances in fundamentals and applications of random fiber lasers

Dmitry V. Churkin,^{1,2,3,*} Srikanth Sugavanam,¹ Ilya D. Vatnik,^{2,3}
Zinan Wang,⁴ Evgenii V. Podivilov,^{2,3} Sergey A. Babin,^{2,3}
Yunjiang Rao,⁴ and Sergei K. Turitsyn^{1,2}

¹Aston Institute of Photonic Technologies, Aston University, Birmingham B4 7ET, UK

²Novosibirsk State University, Pirogova, 2, 630090 Novosibirsk, Russia

³Institute of Automation and Electrometry, 630090 Novosibirsk, Russia

⁴Key Laboratory of Optical Fiber Sensing & Communications, University of Electronic Science & Technology of China, Chengdu, Sichuan 611731, China

*Corresponding author: d.churkin@aston.ac.uk

Received April 23, 2015; revised June 22, 2015; accepted June 22, 2015; published August 10, 2015 (Doc. ID 239686)

Random fiber lasers blend together attractive features of traditional random lasers, such as low cost and simplicity of fabrication, with high-performance characteristics of conventional fiber lasers, such as good directionality and high efficiency. Low coherence of random lasers is important for speckle-free imaging applications. The random fiber laser with distributed feedback proposed in 2010 led to a quickly developing class of light sources that utilize inherent optical fiber disorder in the form of the Rayleigh scattering and distributed Raman gain. The random fiber laser is an interesting and practically important example of a photonic device based on exploitation of optical medium disorder. We provide an overview of recent advances in this field, including high-power and high-efficiency generation, spectral and statistical properties of random fiber lasers, nonlinear kinetic theory of such systems, and emerging applications in telecommunications and distributed sensing. © 2015 Optical Society of America

OCIS codes: (060.3510) Lasers, fiber; (140.3490) Lasers, distributed-feedback; (140.3510) Lasers, fiber; (280.0280) Remote sensing and sensors

<http://dx.doi.org/10.1364/AOP.7.000516>

1. Introduction	518
2. High-Power and High-Efficiency Generation	519
3. Spectral, Temporal, and Statistical Properties of Random Fiber Laser Generation	525
3.1. Managing Spectral Performance of Raman-Gain-Based Random Fiber Lasers	525

3.2. Spectral Properties of Random Fiber Lasers of Other Types	531
3.3. Temporal Dynamics and Statistical Properties	536
4. Theoretical Description of Spectral Properties of Random Fiber Lasers	540
4.1. Linear Spectral Narrowing Near the Generation Threshold	540
4.1a. Numerical Simulation of Spectral Narrowing within the Modified Power Balance Model	540
4.1b. Spectral Narrowing within the Modified Schawlow–Townes Approach	543
4.2. Nonlinear Kinetic Spectral Broadening	545
4.2a. Principles of the Wave Kinetic Approach in Application for Random Fiber Lasers	545
4.2b. Experimental Verification of Nonlinear Kinetic Theory Predictions	549
5. Applications	551
5.1. Random Fiber Laser for Telecommunication Applications	551
5.2. Random Fiber Laser as a Remote Point-Based Sensing System.	553
5.3. Random Fiber Laser for Applications in Distributed Sensing	557
6. Discussion	558
Acknowledgments	560
References	560

Recent advances in fundamentals and applications of random fiber lasers

Dmitry V. Churkin, Srikanth Sugavanam, Ilya D. Vatnik,
Zinan Wang, Evgenii V. Podivilov, Sergey A. Babin,
Yunjiang Rao, and Sergei K. Turitsyn

1. Introduction

Materials with periodically structured refractive indices play very important roles in optical science and technology. The optical characteristics of periodic and quasi-periodic photonic structures are exploited in a range of devices and technologies: filters [1], photonic crystal fibers [2], fiber Bragg gratings [3,4] and distributed feedback (DFB) lasers based on long gratings inscribed in active or passive fibers [5,6], enhancement of nonlinear effects [7–9], realization of negative refractive index materials [10], optical memory, light delay lines, and even in the observation of photonic analogues of quantum mechanics [11]. However, a majority of naturally occurring changes of refractive index in media arise from random density fluctuations, which predominantly result in random scattering of light. Generally, random fluctuations are undesirable and special measures are usually taken to avoid their emergence, such as minimizing atmospheric turbulence by means of adaptive optics in telescopes [12] and periodic or distributed amplification in optical fiber communication links to compensate for Rayleigh scattering losses of the propagating signal [13].

A very different, counterintuitive approach is to explore how disorder of refractive index can be translated into new optical technologies and devices. Many naturally existing photonic structures exhibit a randomness in their periodicity, but they can surpass manmade periodic structures in optical performance [14]. These properties give the notion that disorder—either naturally occurring (like in submicrometer irregularities of glass) or artificially introduced—can in fact contribute toward an enhanced functionality of photonic devices (see for example, [15,16]), a notion that has fueled growing interest in the development of engineering design rules for photonic devices based on disorder.

The random laser is an addition to this ever-growing list of disorder-based photonic devices. When one thinks of a laser, the picture that comes to mind is one of an optical resonator encapsulating a gain medium. The optical resonator forms an important part of the laser, which provides the spectrally filtered feedback necessary for the onset of lasing, and often employs active stabilization procedures for optimal operation. In contrast, in a random laser, the feedback is generated via multiple scatterers interdispersed with gain media, distributed randomly over space and/or time. The transport properties of light in this random medium can then be controlled by altering the concentration and dimensions of the scattering particles in such a way that its mean free path becomes much longer than the amplification length. In this scenario, one can envision an incoherent feedback mechanism, where the scattered light is amplified by the spectrally dependent gain, giving rise to a spectral narrowing of radiation.

Alternatively, the scattered paths might close onto themselves, giving rise to constructive interference, which could in turn set up several microscopic lasers within the random medium. The phenomenon of random lasing was first observed by Ambartsumyan *et al.* [17], who replaced one of the mirrors of a ruby laser with a diffusive surface, giving rise to incoherent feedback. Since then, random lasing has been realized in several configurations—colloidal solutions [18], powdered laser crystals [19], zinc oxide powders [20], and even in biological tissues [21] and cold atoms [22]. A comprehensive review of the field in general is beyond the scope of the current work, and the reader is referred to excellent reviews of the field by Cao *et al.* [23,24] and citations therein. The relative simplicity of the realization of such lasers holds tremendous potential for practical applications, particularly if the disorder is of natural origin (e.g., one arising from a self-organization process), and does not need to be prefabricated.

A novel type of random laser—the random DFB fiber laser—was recently reported [25]. Randomly distributed refractive index inhomogeneities throughout the length of the fiber give rise to scattering, whence a fraction of the scattered light is recaptured and amplified, giving rise to the necessary feedback process [26]. Conventional optical fiber is used as a transport medium, while the gain is established via stimulated Raman scattering (SRS). Such a system intrinsically provides directionality, thus making it a viable solution for commonplace laser applications. Starting from the first demonstration in 2010, random DFB fiber lasers have received much research attention, which has resulted in a range of practically important devices. The principle of operation of random DFB fiber lasers and various technical designs are reviewed in [26]. In the current paper we review recent advances in the field and focus on the ultimate power and efficiency performance of the laser, managing its spectral properties in experiments, and fundamental challenges in theoretical description of such sources.

2. High-Power and High-Efficiency Generation

Due to the relatively low Rayleigh backscattering coefficient, random lasing in a single-mode fiber (SMF) can be more easily achieved if a high pump power and/or a long fiber is used. In early experiments, quite a long fiber ($L > 40$ km) was applied to enhance the integral value of the random Rayleigh DFB and Raman gain, thus achieving random lasing with relatively low pump power (~ 1 W) [25,27]. On the other hand, generation efficiency of a random laser based on such a long fiber appears to be sufficiently lower than that in a conventional Raman fiber laser with optimal cavity design. So, one of the most important directions of random fiber laser development is efficiency enhancement.

Just after the first experiments, it became clear that shorter fibers and shorter operating wavelengths (which are characterized by higher Rayleigh backscattering as well as Raman gain coefficients) are preferable for high-efficiency generation in random fiber lasers, in spite of higher threshold pump power in this case; see [28,29]. An exponential growth of efficiency with decreasing length was predicted analytically [28] for the initial random fiber laser configuration with two fiber arms symmetrically pumped by two pump sources from the center [25]. Later on, various pumping schemes, both symmetric and asymmetric, in combination with insertion of broadband or spectrally selective reflectors at one fiber end were also tested to find the optimal configuration; see [26] for a review. These endeavors resulted very recently in demonstration of high-power

random distributed feedback (DFB) fiber laser operation (in the 10–100 W range) with ultimate efficiency (close to the quantum limit), which has attracted a lot of attention; see [30] and citations therein. Thus a new direction of high-power laser source development has been initiated. The results obtained in this direction will be reviewed in more detail here.

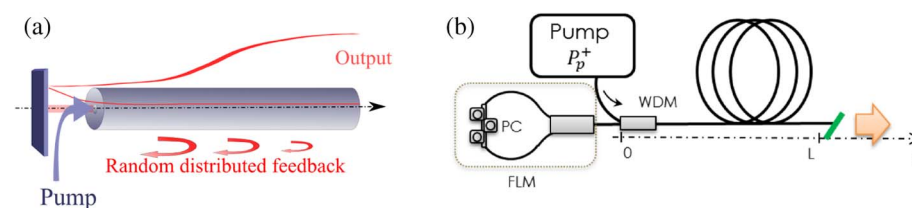
The basic scheme of a random fiber laser with one-side pumping is shown in Fig. 1(a). The pump source is coupled to the fiber at one end, thus providing distributed Raman gain for the Stokes wave at redshifted wavelength (relative to the pump). The Rayleigh backscattered radiation is used as random DFB, resulting in lasing at the Stokes wavelength. The fiber ends are cleaved at an angle of $>10^\circ$, which prevents Fresnel reflection. The lasing threshold is reached when the pump-induced integral gain for the Stokes wave becomes higher than the integral round-trip losses, which are defined mainly by the Rayleigh scattering outside the fiber waveguide.

There can be different technical realizations of the random fiber laser concept. In the first demonstration [25], a piece of fiber was symmetrically pumped from the central point (over length) of the fiber span in two opposite directions. The threshold pump power may be sufficiently reduced if one inserts a highly reflecting mirror at one side and uses only one pump laser, as schematically shown on Fig. 1(b). Despite use of the mirror in this configuration, the laser generation properties are still defined by the random DFB. In terms of its properties, the symmetrical configuration with no mirrors [25] and the configuration shown on Fig. 1 are identical (see [26] for details), so for the remainder of this review we do not distinguish between them. The mirror can be placed at different positions relative to the pump wave coupling point. If the mirror is placed near the pump-coupling end, as shown in Fig. 1, the output Stokes wave reflected by the mirror copropagates with the pump wave and reaches its maximum power near the fiber end. Such a configuration is conventionally called forward pumped, as opposed to the backward-pumped one in which the mirror is placed at the opposite end of the fiber. The random fiber laser configuration with no mirrors and only one pump from the fiber end is called a single-arm configuration.

The generation power and generation efficiency of the random fiber laser can be described within a simple power balance model:

$$\begin{cases} \pm \frac{dP^\pm}{dz} = -\alpha_p P^\pm - g_R \frac{\omega_p}{\omega_s} P^\pm (I^- + I^+), \\ \pm \frac{dI^\pm}{dz} = -\alpha_s I^\pm + g_R (P^+ + P^-) I^\pm + \epsilon I^\mp. \end{cases} \quad (1)$$

Figure 1



(a) Basic scheme of the forward-pumped high-power RDFBL (reprinted with permission from Ref. [30]; copyright 2014 Optical Society of America). (b) The experimental setup in forward-pumped configuration. Reprinted with permission from Vatnik *et al.*, *Laser Phys. Lett.* **11**, 075101 (2014), Ref. [31]. Copyright IOP Publishing. All rights reserved.

Here P denotes the power of the pump wave and I denotes Stokes wave power, lower indices p and s refer to the pump and Stokes waves, respectively, while upper indices $+$ and $-$ refer to the forward (propagating in the direction along the z axis) and backward (corresponding to the z axis) propagating waves, respectively. Coefficient α defines the linear attenuation, g_R is the gain coefficient at the wavelength with maximal Raman amplification, and ε is the backscattering coefficient, $\varepsilon = Q\alpha_s$, where $Q \sim 1/600$ is a backscattered factor [26].

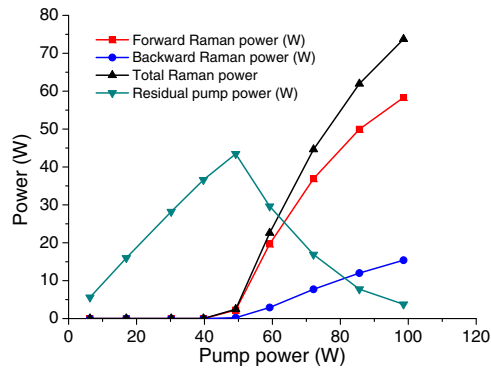
The power balance equation set in Eqs. (1) is the simplest model of the random fiber laser and does not include spectral properties or nonlinear effects. Despite that, it proved to provide precise description of the generation power, the generation threshold, and the generation efficiency of a random fiber laser [26]. The spectral properties and contribution of nonlinearity will be rigorously described in Section 4.

The performed numerical analysis of Eqs. (1) in the case of a single-arm configuration where $P^- = 0$ [29] with corresponding boundary conditions revealed that the output power of the forward propagating Stokes wave is always lower than the output power of the backward Stokes wave; see also [26]. The backward wave output power depends always linearly on pump power, and the forward output power would be saturated with the increase of pump power. The reason is that in the single-arm configuration, the backward wave is amplified mainly near the pump-coupling fiber end where the pump wave is undepleted, whereas the forward wave would propagate in the remaining fiber part, where the Raman gain may not compensate the linear attenuation due to the pump depletion. As a result, the slope efficiency for a forward-propagating Stokes wave exponentially decreases with increasing length, whereas the backward wave efficiency is nearly constant, approaching maximum value of 90% at $L \rightarrow 0$. Herewith, maximum single-end output power and absolute optical efficiency ($\eta \sim 0.8$) is reached for the backward wave in a long enough ($L \geq 15$ km) random fiber laser.

It was also found that even tiny ($\sim 10^{-4}$) parasitic point reflections on fiber ends could significantly change the power performance of the RDFBL in the single-arm configuration. In such a case, the power of the forward wave can become higher than the power of the backward wave. Nevertheless, in such a configuration with a 300 m SMF [32], output power of as high as 73.7 W was achieved with absolute optical efficiency of about 75%; see Fig. 2, where the power value is a sum of forward and backward ones. Here the forward component is almost 4 times higher than the backward one, which indicates the presence of parasitic reflections. The demonstrated laser is pumped at 1120 nm and generates at 1184 nm. Note that in real applications, the parasitic reflections could easily be introduced into the system because of dirt/dust on fiber ends, fiber connectors, etc., which would limit the application range of the single-arm configuration in high-power regimes. In this sense, the random fiber laser configuration based on half-open cavities with one highly reflecting mirror is more practical from the point of both minimizing parasitic reflection influence and concentrating all output power into one fiber end.

The forward-pumped random fiber laser configuration, which has a point reflector at the pump-coupling side of the fiber span [see Fig. 1(b)], was initially proposed for the purpose of reducing the threshold pump power. The inverse exponential dependence of the output efficiency on the fiber length predicted

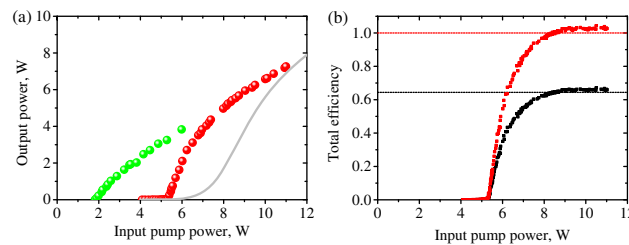
Figure 2



Experimental demonstration of high-power operation of the random fiber laser. The generation power in the forward and backward directions is shown by red and blue symbols, respectively. The total generation power is shown by black symbols. The power of the residual pump wave is shown by green symbols. Reprinted from Zhang *et al.*, *Laser Phys. Lett.* **11**, 075104 (2014), Ref. [32]. Copyright IOP Publishing. Reproduced with permission. All rights reserved.

in [28] indicates that high optical conversion efficiency can be achieved with short fiber length. Recent experiments on a short-fiber forward-pumped random fiber laser based on a fiber loop mirror made of a 3 dB coupler proved this prediction [31,33]. With a 850 m long phosphosilicate fiber featuring a large Stokes shift, of first-order random lasing operating at 1308 nm achieved 7.3 W of power with 66% optical conversion efficiency at 1115 nm pump radiation [31]. After the pump power reaches the threshold, the differential generation efficiency demonstrates extraordinary behavior: just above the threshold, it amounts to several hundred percent, and more than 2 W of the lasing is generated from 0.5 W of pump excess over the lasing threshold; see Fig. 3(a). As the threshold pump power is $P_{\text{th}} = 5.5$ W, 2 W of output power is generated from the 6 W of total pump power launched into the fiber, so there is no violation of energy conservation law. Moreover, the corresponding quantum efficiency can exceed 100%, due to the specific longitudinal power distribution along the cavity and lower loss for the generated wave compared to the pump wave [31]; see Fig. 3(b). The *relative* quantum efficiency is defined here as the ratio of the Stokes photons, $N_S^{\text{out}} = P_S^{\text{out}}/h\nu_S$, to the pump photons in a loss-only regime at the cavity output, $N_P^{\text{out}} = P_P^{\text{in}}e^{-\alpha_p l}/h\nu_P$. Note that the *total* quantum efficiency [black line in Fig. 3(b)], which is the ratio of generated photon number to injected pump photon number, can never be higher than 100% (actually, it cannot be higher than the loss level).

Despite an extremely small value of the integral Rayleigh backscattering coefficient (10^{-4}), random DFB has a crucial role on the generation performance of a short random fiber laser. Indeed, if the feedback is organized in the conventional way by reflecting sufficient part of the radiation from the point-action mirror, the output efficiency as well as the output power deteriorates. In the case of 4% Fresnel reflection from the normally cleaved fiber end [see Fig. 3(a)], despite the lower generation threshold, the maximum output power is much lower compared with pure random lasing because of the cascaded second Stokes wave generation that starts at pump power levels of more than 5.5 W. Another limiting case is a system without any feedback, neither randomly distributed nor

Figure 3

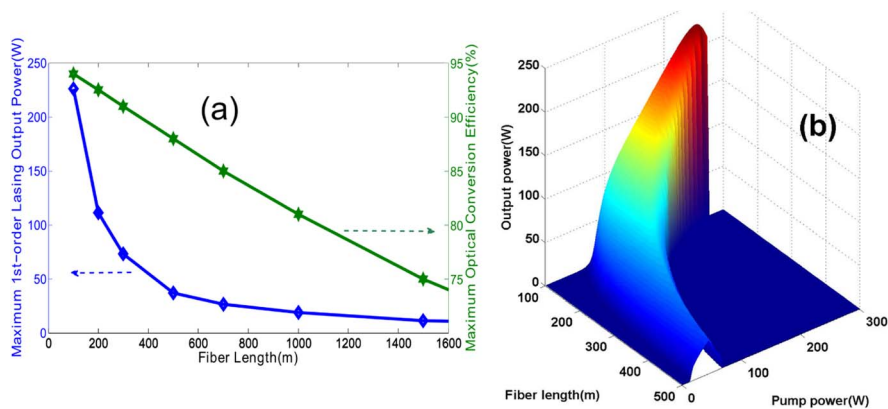
Ultimate generation efficiency of the random fiber laser. (a) Experimentally measured output power of the random fiber laser (red points) compared with the output power of the laser having a 4% output reflector (green points). Results are compared with the numerically calculated output power of an ASE source (gray line) of the same length (i.e., the system without random DFB). (b) Total optical efficiency (black squares, defined as the ratio of the output generation power to the input pump power) and relative quantum conversion efficiency (red squares, defined as the ratio of the generated photon number at the laser output to the transmitted pump photon number if the Raman conversion is absent) in comparison with theoretical limits in approximation of equal attenuation of the pump and Stokes waves (dashed lines). Reprinted with permission from Vatnik *et al.*, *Laser Phys. Lett.* **11**, 075101 (2014), Ref. [31]. Copyright IOP Publishing. All rights reserved.

conventional point-action reflection. Indeed, simulations show that, at high powers (10 W), an efficient pump-to-Stokes conversion may also occur in a single pass without any feedback in the regime of amplified SRS [see Fig. 3(a)], but spectral features in this case are quite different from that for a random fiber laser (which will be discussed in later sections).

Reference [33] presents a comprehensive study on a highly efficient forward-pumped random fiber laser with a half-open cavity based on 1 km of standard SMF operating at 1140 nm under 1090 nm pumping. The results also show that shorter fiber lengths allow improvement of the optical conversion efficiency of first-order random lasing by suppressing the generation of second-order random lasing at high pump power. The absolute optical conversion efficiency can approach the quantum limit (defined as $h\nu_S/h\nu_P$), showing the ultimate efficiency; see Fig. 4. As expected, the power performance in a forward-pumped random fiber laser is insensitive to parasitic reflection on the fiber end. This characteristic is important for ensuring laser performance in practical experimental conditions.

The effect of point reflectors' reflectivity on the characteristics of a high-power forward-pumped random fiber laser was investigated in [34]. With 500 m of SMF, the maximum achievable first-order random lasing output can even be increased if the reflectivity of the mirror is decreased from 0.9 to 0.01. Numerical analysis is based on Eqs. (1) (with corresponding boundary conditions for the forward-pumped configuration). The results show that a mirror with low reflectivity is preferable in order to achieve higher output power, and even with a flat fiber end, which has $\sim 4\%$ broadband reflection, could be sufficient. Therefore, a forward-pumped random fiber laser can be easier to construct for various lasing wavelengths, and the configuration is much simpler, making the forward-pumped high-power random fiber laser very attractive in real applications. Furthermore, efficient cascaded random lasing in a forward-pumped

Figure 4



(a) Maximum output power and optical conversion efficiency of the first-order random lasing as a function of fiber length. Results of numerical calculation within the power balance model are shown. Copyright 2015 IEEE. Reprinted, with permission, from Wang *et al.*, IEEE J. Sel. Top. Quantum Electron. **21**, 0900506 (2015) [33]. (b) Output power versus input pump power for different fiber lengths. Numerical simulations.

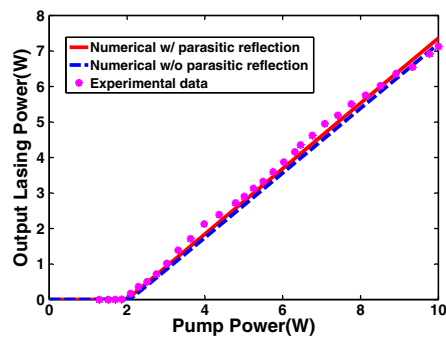
random fiber laser has been demonstrated in [35]. The fiber loop mirror provides the feedback for both the first- and second-order Stokes waves. As a result, output power for the second Stokes component exceeds 5 W at pump power of 11 W.

In the backward-pumping scheme, low-threshold high-efficiency operation of the random fiber laser can be obtained, featuring a linear output [36]. With a point-reflector placed at the far end of the fiber (opposite to the pump-coupling point), most energy is further pushed toward the pump side, comparing with the single-arm scheme, producing high-efficiency output into the open fiber end. Also, the influence of the parasitic reflection can be significantly suppressed here. As both the threshold and the slope efficiency depend on the fiber length, the fiber length should be carefully chosen for the purpose of achieving low-threshold and high-power random lasing simultaneously. In contrast to the forward-pumped random fiber laser, the output power increases linearly with the pump power after the threshold, making the backward-pumped random fiber laser's configuration an alternative way to generate high-power laser radiation for practical applications. As experimental verification, a low-threshold (2 W), high-power (7.13 W output at 10 W pump), high-efficiency (more than 90% slope efficiency) random fiber laser with linear output at 1145 nm is achieved, as shown in Fig. 5.

Note that other fiber types can be used in random fiber lasers, resulting also in changes of power and efficiency performance. For example, random lasing was demonstrated in a nitrogen-doped silica fiber with a fiber span of just 500 m with an efficiency of 58% [37]. The nitrogen-doped fiber is characterized by the higher values of Rayleigh scattering and Raman gain ($7.5 \text{ W}^{-1} \text{ km}^{-1}$).

In all the treated schemes, pumping is produced by the laser radiation, e.g., generated by a high-power Yb-doped fiber laser. For practical applications it is important to further simplify the pumping scheme by implementing direct pumping of a random fiber laser by high-power laser diodes. Such an endeavor

Figure 5



Linear output power dependence of the random fiber laser. Copyright 2015 IEEE. Reprinted, with permission, from Fan *et al.*, IEEE Photon. Technol. Lett. **27**, 319–322 (2015), Ref. [36].

was attempted in [38], where random lasing was achieved in a 4.5 km multimode gradient-index fiber directly pumped by a high-power multimode laser diode at 940 nm. Lasing was obtained at 980 nm when the coupled pump power exceeded 40 W. Since the maximum pumping was limited by 45 W, the generated power approached the 1 W level only, but the differential efficiency was high enough to obtain a higher output power at higher excess above the threshold. In addition, this scheme has a prominent feature that enables radical beam quality improvement. The measured divergence of the output beam at 980 nm is 4.5 times lower than that of the pump beam. In addition to the well-known Raman clean-up effect based on the radial-coordinate-dependent Raman gain in gradient-index multimode fibers, Rayleigh-scattering-based feedback may also have some impact on the clean-up due to the radial variation of the refractive index (and its fluctuations, as well). It has been indirectly confirmed in experiments with linear-cavity Raman lasers with the same fiber [39] that the observed divergence of the output beam was 1.5 times larger than that for the Rayleigh-scattering-based feedback scheme. This approach seems to be attractive for high-power generation in the short-wavelength spectral domain ($<1 \mu\text{m}$), where generation of rare-earth-doped fiber lasers is problematic. For example, by using a commercially available high-power laser diode around 800 nm, one can generate in conventional multimode passive fibers a high-quality beam around 830 nm [40].

Combination of the approach of direct laser diode pumping with efficient all-fiber design of a random fiber laser with a short half-open cavity seems to be a promising way for development of highly efficient laser sources operating on various wavelengths in a broad spectral range (from below $1 \mu\text{m}$ to above $2 \mu\text{m}$) in a simple and reliable all-fiber configuration based on passive fibers and high-power laser diodes only, thus offering new applications of random fiber lasers.

3. Spectral, Temporal, and Statistical Properties of Random Fiber Laser Generation

3.1. Managing Spectral Performance of Raman-Gain-Based Random Fiber Lasers

The spectral properties of the radiation of random DFB fiber lasers are of great interest and practical importance. A wide range of random fiber lasers with

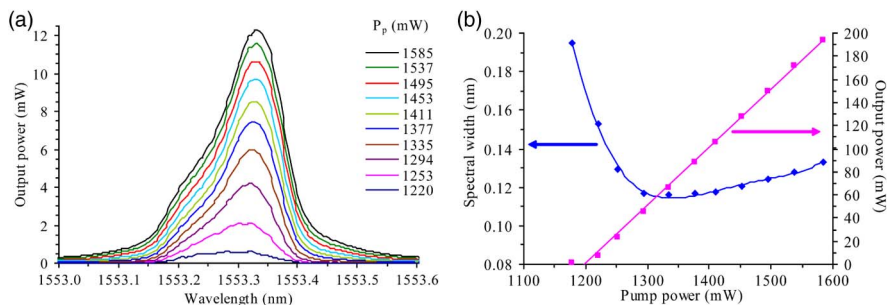
substantially different spectral performance have been recently developed. In a random DFB fiber laser of standard configuration (without any special measures to tailor spectral properties), the generation spectrum is defined by the Raman gain profile of the fiber used. The generation occurs at frequencies at which the Raman gain spectral profile has local maxima. If conventional fiber is used in which the Raman gain has two local maxima, the generation spectrum can often have a shape of two separated broad bell-shaped peaks; see [26] for details. In random DFB fiber lasers based on phosphosilicate fiber, the generation spectrum has the form of a single bell-shaped peak, as the Raman gain profile has a one local maximum only [41].

The typical generation spectrum of a Raman fiber laser is bell shaped [Fig. 6(a)]. However, the spectrum shape strongly depends on the pump and generation power. At low pump power (just below the generation threshold), the spectral shape is close to the Raman gain spectral profile, and it deviates from this shape at higher pump power. While pump power increases, the spectrum becomes narrower [Fig. 6(b)]. However, at higher pump power, the spectral broadening starts to prevail. The spectrum of a random fiber laser is modeless as the laser has no cavity of fixed length. This fact was directly confirmed in experimental measurements of the mode structure in [28].

The spectral broadening law could depend on the random fiber laser configuration. For example, as shown in [42], in a forward-pumped configuration, the spectral width increases linearly over the pump power. If the laser setup incorporates a point-based mirror, the spectral broadening rate depends on the reflectivity of such mirror: the higher is the reflection coefficient of the mirror, the broader is the generated spectrum, [42]. Such dependence could be connected with the fact that power characteristics (generation threshold, generation efficiency, and longitudinal power distribution) are changed when the reflection coefficient of the point-based mirror in the random fiber laser is changed [34]. This could lead to different levels of generation power at the same pump power level, which in turn affects the width of the generation spectrum. Indeed, it is assumed that at high power the spectrum is influenced by nonlinear processes that are intensity dependent; see Section 4.2 for details.

The spectral characteristics of random fiber lasers can depend on the type of the fiber used.

Figure 6



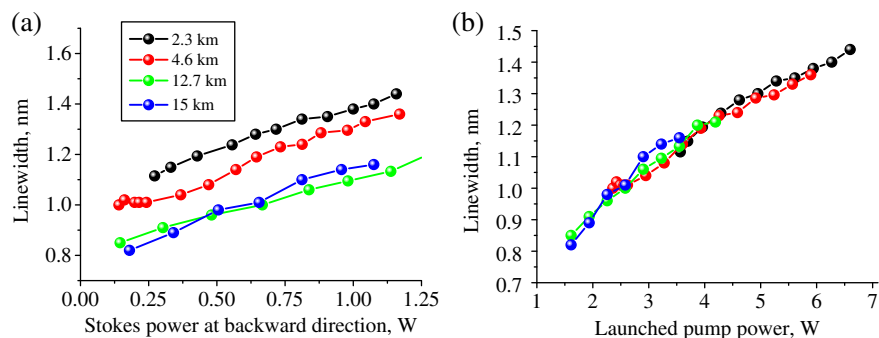
Typical generation spectrum of the 51 km long random DFB fiber laser under 1455 nm pumping. (a) Spectral shape at different pump power levels, and (b) spectral width as a function of generation power. Reprinted with permission from Ref. [42]; copyright 2011 Optical Society of America.

However, variation of spectral width could be associated not only with fiber parameters, but also with the length of the laser. In particular, in [43], experimental study of the dependence of spectral properties of a random DFB fiber laser on the laser's length was presented. The laser's length was varied from 2 to 15 km. The laser was pumped at 1064 nm, which resulted in generation near 1118 nm. An increase of the fiber length resulted in a decrease of the laser generation threshold pump power, while the slope efficiency was almost constant. The longer the laser, the narrower the generation spectrum (at fixed generation power) [Fig. 7(a)]. Because the generation threshold and efficiency are different in lasers of different lengths, the same generation power could be achieved at different pump powers. It is interesting that, if the spectral width is plotted as a function of pump (but not generation) power, then the spectral width remains the same for any cavity length Fig. [7(b)].

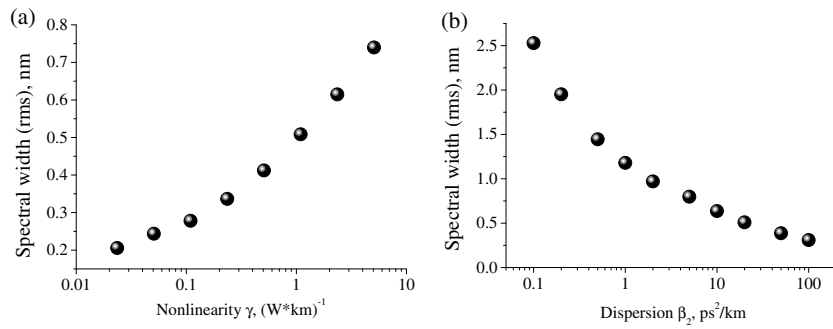
The strong dependence of the spectral properties of random fiber laser generation on fiber parameters were found recently in numerical calculations [44]. In that paper, full numerical nonlinear Schrödinger equation (NLSE)-based modeling of the generation properties of random DFB fiber lasers is reported. As the model takes into account dispersion and nonlinearity, one can track their influence on the spectral properties of random generation. In particular, if the dispersion is fixed, but nonlinearity is increased, the generation spectrum becomes broader [Fig. 8(a)]. However, the spectrum becomes narrower in lasers made of fiber with higher dispersion [Fig. 8(b)]. This means that proper dispersion and/or nonlinear management could be a practical tool to change the spectral properties in real random DFB fiber laser systems. In this regard, we have to note that how the spectral properties of random DFB fiber lasers depend on system parameters is yet to be experimentally investigated. Preliminary studies show that in a random fiber laser made of 1060-XP fiber, the spectrum is broader (around 1.5 nm) than in a laser based on TrueWave fiber (below 1 nm). The spectral broadening law could also be different: The spectral width almost does not depend on generation power in a random laser based on 1060-XP fiber, while strong dependence is observed in a laser based on TrueWave fiber, [45].

The spectral properties of a random DFB fiber laser can be different if the laser is pumped by linearly polarized radiation. All the lasers reported above have been pumped by unpolarized sources. By using a polarized pump, partially polarized

Figure 7



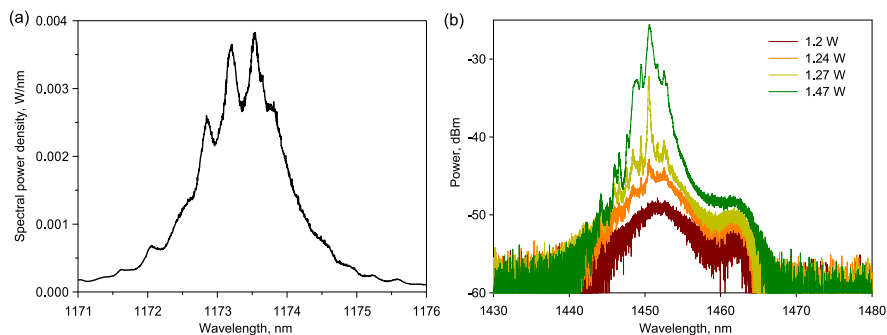
Experimentally measured dependence of the width of the random DFB fiber laser generation spectrum on the laser length. (a) Spectral width as a function of generation power, and (b) spectral width as a function of pump power.

Figure 8

Width of the generation spectrum of a random DFB fiber laser numerically calculated within the NLSE-based model for fiber having different (a) nonlinearity and (b) dispersion. Reprinted with permission from Ref. [44]; copyright 2013 Optical Society of America.

generation could be obtained with a generation spectrum exhibiting discrete narrow spectral feature, in contrast to the smooth spectrum observed for depolarized pumping. The first indication of that was reported in [46], in which a spiky generation spectrum was observed in a short random fiber laser operating in the 1 μm spectral range under polarized pumping [Fig. 9(a)]. A much more detailed study was reported in [47] [Fig. 9(b)]. It was found that the threshold, output power, degree of polarization, and the state of polarization (SOP) of the lasing can be significantly influenced by the SOP of the pump. Because the Raman gain is different for orthogonal polarizations, the longitudinal power distributions are different in the case of polarized and depolarized pumping, which results in considerable reduction of the generation slope efficiency for polarized radiation. However, it is still unclear why narrow lines appear in the generation spectrum under polarized pumping. Further investigation is needed in this direction.

Spectral management could be performed by incorporation into the cavity of the random fiber laser different spectral elements (for example, filters) and tailoring

Figure 9

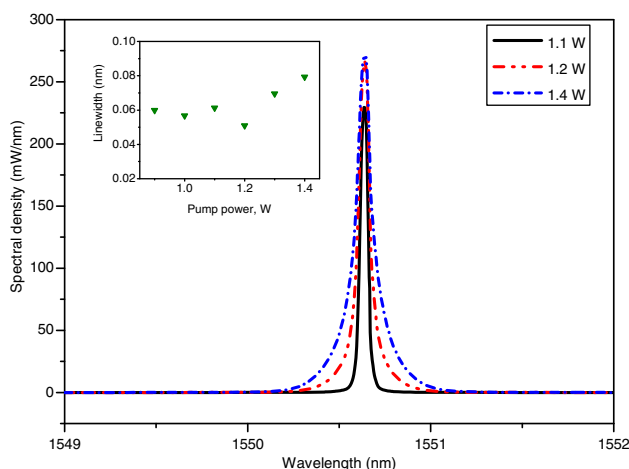
Generation spectrum of the random DFB fiber laser pumped by a polarized pump source. (a) The laser operating in the 1 μm spectral range. Reprinted with permission from Churkin *et al.*, *Laser Phys.* **21**, 1525–1529 (2011), Ref. [46]. Copyright IOP Publishing. All rights reserved. (b) The laser operating in the 1.45 μm spectral range. Reprinted with permission from Wu *et al.*, *Laser Phys. Lett.* **12**, 015101 (2015), Ref. [47]. Copyright IOP Publishing. All rights reserved.

their spectral properties. The specific highly nonuniform longitudinal distribution in long random DFB fiber lasers [48] allows management of the spectral properties of high-power output radiation by means of placing low-power-handling spectral components into a specific point over the cavity of the random fiber laser, where the generation power is low. In this way [49], narrowband generation has been demonstrated in which a narrowband spectral filter (fiber Bragg grating or Fabry–Perot etalon) has been inserted via a set of circulators into the symmetrical configuration of a random fiber laser made of spans of 40 km standard Corning SMF 28. The linewidth of the output radiation is around 0.05 nm [Fig. 10], which corresponds to the spectral width of the spectral filter used. Let us recall that the typical spectrum width in a random fiber laser without spectral filters is around 1 nm [Fig. 6].

Note that if the spectral filters are tunable, then tunable generation of random DFB fiber lasers can be demonstrated. Tunability in a random fiber laser was first demonstrated in [28] by the use of a simple filter in the symmetric pump configuration. An extremely flat tuning curve over the whole gain spectrum of the laser was demonstrated in this very simple configuration. Further works on tunable random DFB fiber lasers include [50,51]. In [52], tunability of a random fiber laser was demonstrated by using long period fiber Bragg gratings. In general, the typical tuning range offered by random DFB fiber lasers is comparable to that offered by conventional Raman fiber lasers. Indeed, while the latter offers tunability of up to 50 nm [53,54], a similar range of 40 nm was demonstrated using random DFB and a tunable filter [28].

Use of spectral filters having multiple transmission peaks or a set of spectral filters results in demonstration of multiwavelength generation [55–60]. The use of multiple fiber Bragg gratings was demonstrated as a viable straightforward route for obtaining multiwavelength generation in random fiber lasers [55,56,61]. Gain competition effects that are usually seen in conventional cavity-based lasers were absent because of the random nature of the feedback, which resulted in a flatter distribution of generation power over the different generation

Figure 10



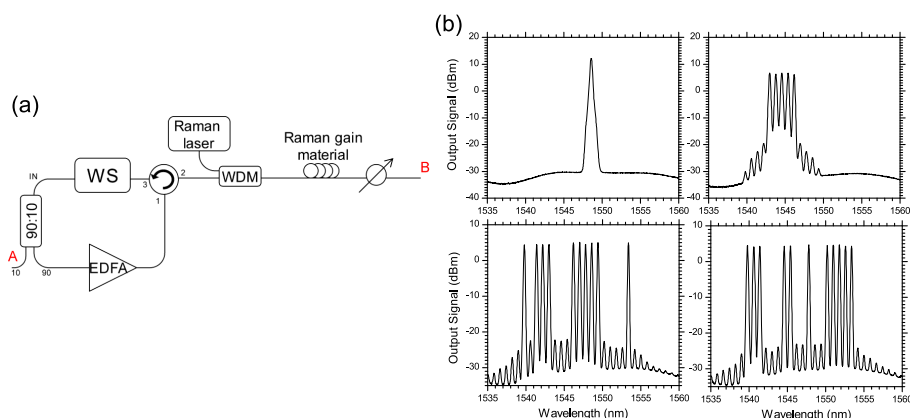
Generation spectrum of the narrowband random DFB fiber laser. Inset: spectral width over pump power. Reprinted with permission from Ref. [49]; copyright 2013 Optical Society of America.

lines. Multiwavelength generation was also demonstrated by the use of an all-fiber Lyot filter [60]. A flat power distribution was obtained, which was attributed to a homogeneous gain saturation mechanism. A much flatter wavelength response was demonstrated by the use of an actively controlled wavelength filter [62]. The output of the laser was monitored continuously and used as feedback for the filter. Multiwavelength lasing over 30 different wavelengths over the International Telecommunication Union (ITU) grid was demonstrated. Furthermore, real-time (on a timescale of filter response time of around 1 s) switching between different wavelengths was also possible in this configuration.

Simultaneous multiwavelength and tunable generation could be also achieved if the multitransmission peak spectral filter could be tuned in some way. For example, multiwavelength and tunable generation in a random fiber laser was demonstrated in [63]. A microprocessed fiber Fabry–Perot filter combined with a Mach–Zehnder interferometer formed by a pair of special long-period fiber gratings was incorporated into the random fiber laser. Tuning was achieved by bending the spectral filter, so the tunable range was limited (from 1553.9 to 1565.4 nm). Zhu *et al.* [51] demonstrated a multiwavelength random fiber laser incorporating a Fabry–Perot filter combined with a long-period grating, which was also tunable over a 10 nm range.

Switchable multiwavelength operation of a random fiber laser was demonstrated in [62,64]. The laser cavity is based on a random distributed mirror and a real-time reconfigurable filter mirror structure [Fig. 11(a)]. The laser generates any combination of wavelengths at the 50 and 100 GHz ITU grid spacings within a 15 nm bandwidth in the C band with a total number of lines of up to 18. The lines could be switched automatically and in real time, featuring high stability, broadband response, reconfigurability, versatility, and high power [Fig. 11(b)]. The switchable multiwavelength RDFBL could be used as a versatile source for interrogation systems in fiber optic sensor applications. However, the switching speed is limited by a filter response time of around 1 s.

Figure 11



Switchable multiwavelength random fiber laser: (a) experimental setup and (b) example of multiwavelength operation on different switchable lines separated by 100 GHz. Reprinted with permission from Ref. [64]; copyright 2014 Optical Society of America.

The spectral location of the lasing can also be tuned by choosing an appropriate pump wavelength. By using Yb-doped fiber lasers as a pump source, generation in the 1 μm spectral range was achieved [45,65,66]. If pumped by a short-wavelength multimode pump source, random lasing at 980 nm was demonstrated [38]. Another possibility is to use higher pump power to initiate the generation of higher order Stokes waves in a random fiber laser and, in this way, achieve a generation in different spectral bands. Generation near 1240 nm, [45], 1300 nm [35], 1550 nm [67–69], and 1670 nm [70] in different configurations of random fiber lasers having single or multiple cascades have been achieved.

Finally, very recently, frequency doubling of the radiation of random fiber lasers was demonstrated [71]. Second-harmonic power of around 100 mW near the 654 nm wavelength was achieved via pumping a periodically poled lithium niobate (PPLN) crystal by high power (up to 7 W) of the output radiation of a random fiber laser. In comparison with second-harmonic generation from conventional Raman fiber lasers, random fiber lasers provide even better performance in stability and efficiency, thus having great potential for imaging and other applications requiring low-coherent visible light.

3.2. Spectral Properties of Random Fiber Lasers of Other Types

The spectral properties of the radiation of random fiber lasers can be managed by using different gain mechanisms apart from Raman gain. The spectral properties of such random fiber lasers differ radically from those of random DFB fiber lasers based on Raman gain.

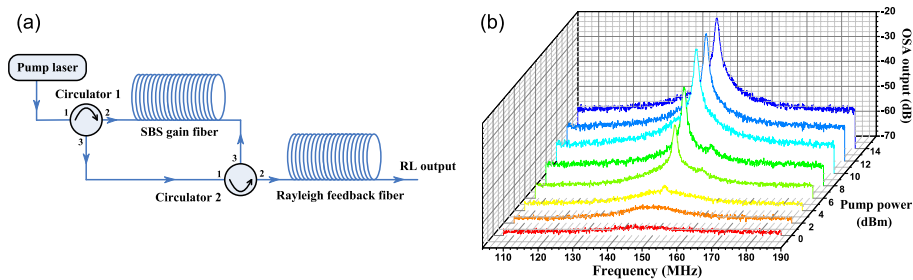
A particular case is the use of stimulated Brillouin scattering (SBS). The typical threshold of Brillouin scattering is 1 order of magnitude lower than that of SRS, which, in fact, leads to observed instabilities before the onset of SRS-based random lasing [25]. The gain bandwidth of SBS is also orders of magnitude narrower, typically of the order of 50–100 MHz, compare with a terahertz bandwidth for the Raman gain. This narrower bandwidth in turn leads to a much narrower lasing linewidth as compared to the random fiber lasers based on Raman gain. SBS-based random lasing was demonstrated in [72–74]. Linewidth narrowing below the SBS gain bandwidth is achieved via the cooperation between Rayleigh scattering and SBS, as shown in [75]. Single frequency lasing with linewidth down to 3 kHz can be achieved (Fig. 12).

Further pump laser instabilities and surrounding acoustic noise resulted in the generation of multiple narrow linewidth peaks, a situation that was remedied by the use of an additional feedback loop employing a narrow linewidth Fabry–Perot etalon [73]. This resulted in frequency stabilization SBS-based random lasing with a spectral linewidth of only 50 Hz [see Fig. 12(b)].

In a recent work, Saxena *et al.* demonstrated a bidirectional pumping architecture [76], which outperforms conventional cavity-based fiber lasers in terms of noise performance. This was attributed to the modeless nature of the random lasing, the polarization sensitive nature of the SBS, and also the contribution of double Rayleigh feedback to linewidth narrowing.

Cooperative SBS and Rayleigh scattering can result in multiwavelength generation if high enough power is generated to initiate cascaded Brillouin processes. Multiwavelength generation in a random fiber laser operating via both Brillouin

Figure 12

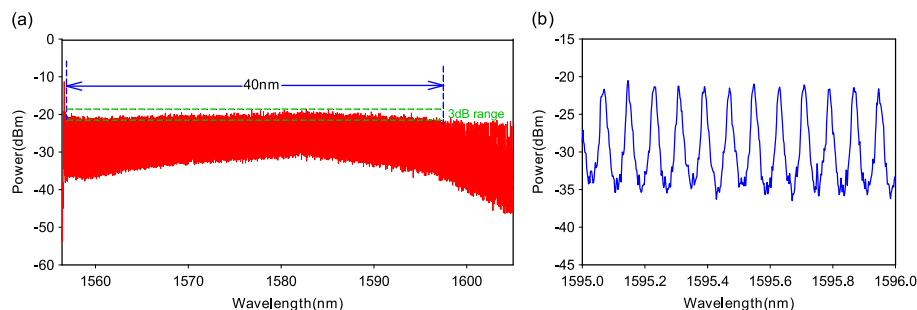


Random fiber laser based on SBS gain: (a) typical experimental realization (reprinted with permission from Ref. [72]; copyright 2013 Optical Society of America) and (b) observed linewidth of frequency-stabilized SBS random lasing with increasing input power (reprinted with permission from Ref. [73]; copyright 2013 Optical Society of America).

and Rayleigh scattering covering a span of 52 nm was achieved in [77,78]. Their experimental setup employed a 11 km span of dispersion-compensating fiber (DCF) seeded with an external cavity laser, while the span was pumped by a combination of a ytterbium fiber laser and Raman pump units near 1450 nm, realizing sixth-order distributed Raman amplification. Thus, very high pump powers (>4.8 W) were required to observe comb generation. The distance between adjacent lines is defined by the SBS frequency shift, i.e., around 11 GHz, which is much less than in multiwavelength random fiber lasers based on Raman gain only. Zamzuri *et al.* [79] demonstrated a similar multiwavelength system, where they used fiber-loop-based feedback to improve the efficiency, allowing generation of the comb at much lower pump powers (500 mW). Martins *et al.* [80,81] used a much shorter span of DCF (1 km) to obtain a 32 nm span. Combinations of different kinds of fiber were also used, which resulted in a better optical signal-to-noise ratio (OSNR) for the peaks [82,83].

A 40 nm wide, flat amplitude Brillouin comb, comprised of 500 individual lines was demonstrated by Wang and co-workers in a Rayleigh-reflection-based configuration [84,85] (Fig. 13). They employed a Raman-amplified DCF for generating the Brillouin–Stokes cascade, together with a 50 km span of standard

Figure 13



Frequency comb generation in a SBS-RS-based random fiber laser. (a) Resulting Brillouin comb spanning over 40 nm. (b) Spectral and power uniformity of even and odd modes in the comb (reprinted with permission from Ref. [84]; copyright 2013 Optical Society of America).

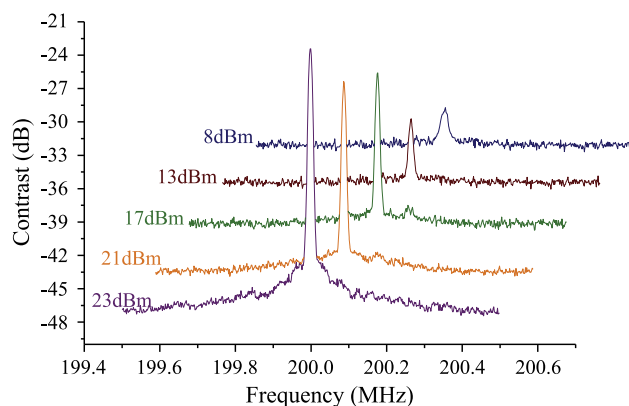
SMF as a distributed mirror for the backward Brillouin–Stokes. The distributed mirror, together with the unique circulator–coupler loop configuration, facilitated multiple reciprocations of both backward (singly scattered) and forward (Rayleigh-assisted doubly scattered Stokes) within the dispersion-compensated fiber. Further, the seeded operation of this configuration led to the realization of a wideband Brillouin comb at much lower powers of the Raman pump and the Brillouin seed, leading to a larger Brillouin comb span, and also to minimization of power and linewidth differences between even and odd modes usually observed in such Brillouin comb lasers [78,82,83,86].

Spectral tuning of the generated combs can be achieved by simply tuning the wavelength of the Brillouin seed and that of the pump. For example, Ahmad *et al.* [86] obtained multiwavelength generation in the S-band region in a 7.7 km span of DCF using Brillouin seeding at 1515 nm and Raman pumps at 1425 nm.

Stimulated Rayleigh scattering has also been demonstrated as a viable mechanism for obtaining random lasing in an optical-fiber-based system [87]; see Fig. 14. The phenomenon is difficult to observe in optical fibers owing to its lower gain and a level of threshold comparable with SBS. Stimulated Rayleigh scattering was first reported in optical fibers by Zhu *et al.* [88], where they observed a linewidth narrowing effect from 10 kHz for the spontaneous Rayleigh to a few kilohertz for the stimulated counterpart. To counteract the effect of SBS, a nonuniform fiber with varying core diameter along its length was used, which raised the effective SBS threshold. The sole gain mechanism operating in this case was the stimulated Rayleigh scattering, which brought about the onset of lasing and results in narrow-linewidth operation of the random fiber lasers.

Random lasers based on the above gain mechanisms act on the principle of distributed amplification, which imposes the need for larger lengths of fiber for sufficient gain and feedback. An alternative approach would be to employ point-based amplification, while using a suitable span of fiber as a passive distributed mirror for nonresonant feedback, analogous to Ambartsumyan’s original experiment [17]. The high gain, wide bandwidth of operation, and low noise figure of erbium-based amplifiers make them an attractive choice for this

Figure 14

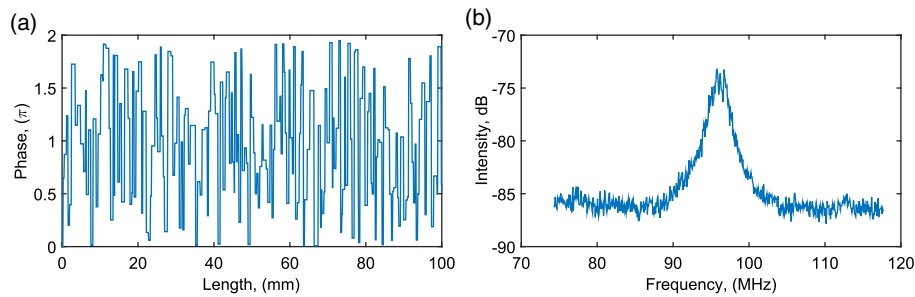


Observed linewidth narrowing with increasing power in a random laser operating via stimulated Rayleigh scattering. Reprinted with permission from “A self-gain random distributed feedback fiber laser based on stimulated Raman scattering,” *Opt. Commun.* **285**, 1371–1374 (2012) [87].

purpose. Passive erbium fibers have been used in combination with the SRS-based random fiber laser configurations to extend the working range of remotely pumped erbium-doped fiber (EDF) to the L band [89]. Further, pumped EDF has been used in the configuration of random fiber lasers to decrease the generation threshold: 50 km of conventional SMF fiber was used to accumulate DFB, which was amplified by the meters-long erbium fiber [90,91]. More recently, Zhang *et al.* [92] studied a combined Raman–erbium-gain-based random fiber laser by incorporating a bidirectionally pumped erbium fiber at the central point of a random fiber laser. The erbium gain lowered the lasing threshold, while the SRS gain allowed for higher power outputs of the order of 100 mW. Competition effects between the two gain mechanisms were also reported.

Multiwavelength generation can be also obtained in random fiber lasers based on combination of gain mechanisms. An erbium–Raman-gain-based multiwavelength random fiber laser was demonstrated by Huang *et al.* [93], who employed a chirped grating on the pump end for broadband reflection and a 50 km span of passive SMF for DFB. The number of comb lines was limited by the grating bandwidth. A combination of SBS and erbium gain can be used to obtain Brillouin comb generation in random fiber lasers [93–96]. For example, Mamdoohi *et al.* [94] demonstrated a 28 nm span of Brillouin comb interspaced by 20 GHz in a configuration employing a span of DCF fiber, followed by a 30 cm long highly doped bismuth oxide erbium fiber. The erbium fiber was pumped by the undepleted pump from the DCF fiber, which then amplified the resulting Brillouin cascades. While the output characteristics highly depended on the values of pump power used for the different components, this configuration resulted in much better noise performance, leading to an OSNR of 28 dB.

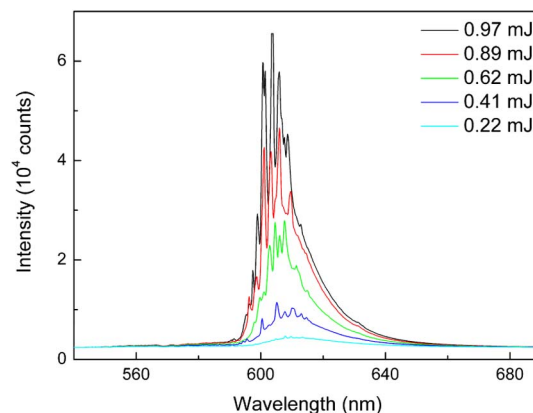
In the above configurations, random lasing was realized by making use of the intrinsic randomness of the fiber medium. It is also possible to artificially introduce randomness within the fiber medium in a controlled fashion, which can in turn provide additional flexibility in tailoring the spectral properties of random lasers. For example, it is known that gratings having randomly distributed phase shifts can exhibit extremely high- Q resonances [97,98]. In [97], light propagation and localization in randomly spaced fiber gratings in a SMF were studied both theoretically and experimentally. The light transmission was measured after each additional grating fabrication and an exponential decay characteristic for the localization theory was demonstrated. In [98], disorder-induced resonances in randomly layered structures have been studied theoretically and experimentally. An algorithm was proposed and developed for the detection and characterization of the effective cavities that give rise to randomness-induced resonances. It was shown in [98] that in an active, amplifying medium, some of the cavities may host lasing modes and the ensemble of lasing cavities may behave as DFB lasers. Artificially introduced randomly located resonant Bragg reflectors (periodic gratings) in a fiber laser system led to typical random lasing in which the resonances revealed themselves through the peaks in the emission spectrum. Gagné and Kashyap [99] demonstrated a distributed Raman fiber laser employing such a random fiber Bragg grating with a linewidth of 430 kHz (Fig. 15). The scheme presented in [99] exploited randomly distributed phase shifts inside a record fiber meter long Bragg grating as a random coherent feedback mechanism. The laser was pumped at 1480 nm and it emitted a CW signal at 1576 nm. The spectral width is limited by the pump noise, and it is believed that a much narrower linewidth is possible in principle [6]. In [6],

Figure 15

Random fiber Bragg grating based Raman fiber laser: (a) typical phase profile of the grating and (b) linewidth of the lasing obtained using a simple end-pumped configuration. Reprinted with permission from Ref. [99]. Copyright 2014 Optical Society of America.

a highly efficient Raman DFB fiber lasers with up to 1.6 W of continuous wave output power was demonstrated. The DFB Bragg gratings of 30 cm length with center π phase shifts were written directly into commercially available passive germano-silica fibers, leading to a narrow linewidth of <0.01 nm at ~ 1117 and ~ 1109 nm. The results presented in [6] demonstrate the possibility of having narrow-linewidth all-fiber laser sources in wavelength bands not traditionally covered by rare-earth-doped silica fibers. Application of random (or quasi-random) fiber gratings may lead to new opportunities for lasing and wave localization based on long structures with strong and broadband reflections [100].

Another methodology for controlling disorder is by way of colloidal suspension of dye and scattering particles within a hollow-core fiber. In such a configuration, the fiber provides the necessary confinement and directionality, while the extent of disorder can be controlled by varying the parameters of the colloidal suspension. Such a configuration was first demonstrated in [101]. The observed spectrum was broad (~ 10 nm), and this was attributed to an incoherent feedback mechanism. More recently, coherent lasing was realized in similar configuration

Figure 16

Coherent lasing using a liquid-filled optical fiber. Figure 2(b) reprinted with permission from Hu *et al.*, “Coherent random fiber laser based on nanoparticles scattering in the extremely weakly scattering regime,” *Phys. Rev. Lett.* 109, 253901 (2012) [102]. Copyright 2012 by the American Physical Society.

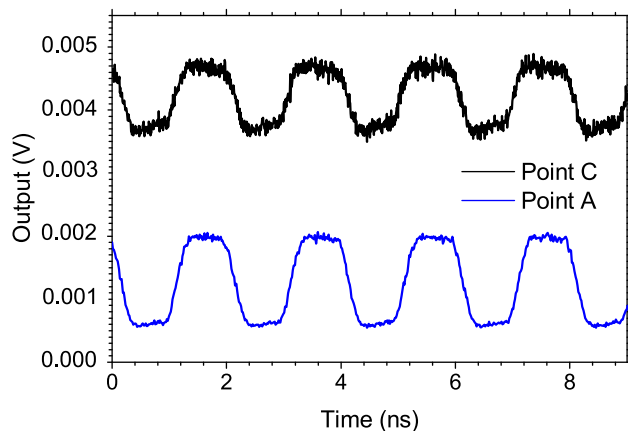
by Hu *et al.* [102], where they used a suspension of polyhedral oligomeric silsesquioxanes (POSS) nanoparticles with the laser dye pyrromethene 597 in CS₂ solution. Multimode lasing was observed near wavelengths of 600 nm, with typical linewidths of the order of 0.9 nm [Fig. 16(a)]. The onset of coherence was attributed to the confinement effect of the waveguide itself, which increased the probability of multiple scattering of the photons within the colloidal suspension. More control over the lasing properties was obtained by embedding the dye and the scattering nanoparticles in a polymer optical fiber in a bottom-up approach [103,104]. More recently, a liquid-filled hollow fiber configuration was used [105] to realize a plasmonic random laser, where they replaced the POSS scattering centers with gold nanoparticles.

3.3. Temporal Dynamics and Statistical Properties

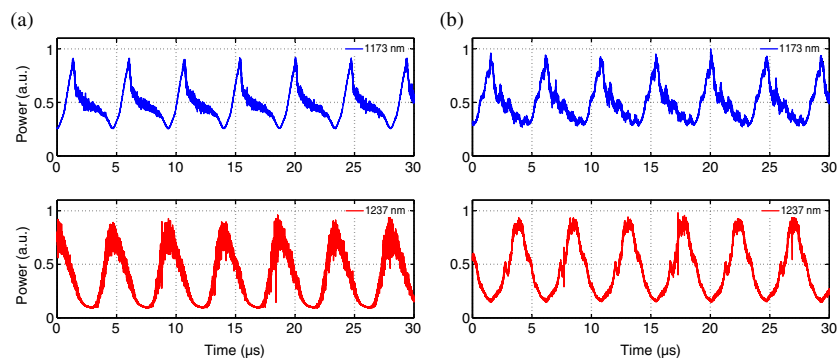
The temporal and statistical properties of laser radiation can be important both for understanding the physical background of the operational mechanism and real-life applications. Here we describe recent experimental efforts to measure temporal and statistical properties of random DFB fiber lasers.

In general, it is known that the random DFB fiber laser is a source of CW radiation: the intensity dynamics of its radiation is almost constant on a millisecond time scale [26]. Such CW output power could be internally modulated by incorporating into the cavity an electro-optical modulator placed into the loop mirror [106]. The modulator has been operated at frequencies up to 500 MHz. As a result, the CW output of the random fiber laser is well-modulated at the same frequency (Fig. 17). Note that the modulation is well-pronounced and synchronous on both ends of the fiber (point A is located near the modulator, and point C is located at the far fiber end). The amount of noise at the laser output (at point C) is higher than the noise level near the modulator. The measured extinction ratio of the modulated random laser is 4 dB higher than the extinction ratio of the modulator used. Note that no fast time fluctuation is resolved in this figure because of the limited bandwidth of the measurement equipment.

Figure 17



Modulated CW output of the random DFB fiber laser incorporating an electro-optical modulator. Reprinted with permission from [106]. Copyright 2013 Optical Society of America.

Figure 18

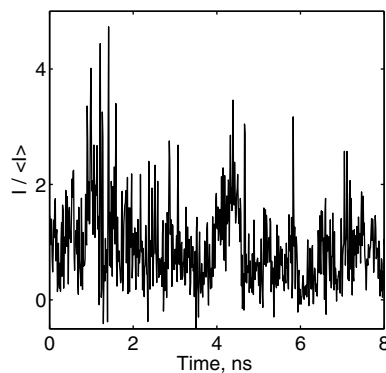
Self-pulsing behavior of the random DFB fiber laser generating simultaneously first (at 1173 nm) and second (at 1237 nm) Stokes waves. Copyright 2014 IEEE. Reprinted, with permission, from Zhang *et al.*, IEEE Photon. Technol. Lett. **26**, 1605–1608 (2014) [107].

Furthermore, in a recent paper [107], slow self-oscillations of the output intensity of a random DFB fiber laser are observed at pump powers above the generation threshold of the second Stokes wave (Fig. 18). The pulses are observed in the time dynamics of both the first and second Stokes waves. The authors use the well-known power balance model to describe the observed temporal oscillations. Note that the laser dynamics can be complex near the generation threshold of the next Stokes component. For example, in [108], effects of on–off and multistate intermitten- cies in a cascaded random fiber laser are experimentally studied near the generation threshold of the second Stokes wave.

We have to also mention the influence of the random DFB via Rayleigh scattering on the temporal properties of a conventional laser with a cavity made from point-based reflectors. For instance, it is known that cooperative RS-SBS based lasers can be made to operate in a Q -switched regime, [109], delivering nanosecond width pulses with peak powers of 1 kW. Similar passive Q switching was also observed in other experiments [110,111], and was explained as an instability effect arising from the second cascade of the SBS [110]. More recently, Rayleigh mediated Q switching was obtained in a thulium-based system, giving rise to 20 ns, 50 mJ pulses in the 2 μ m wavelength region [112].

Slow oscillations in the output power or the possibility of internally modulating the laser output are not, however, related to intrinsic fast intensity fluctuations of the intensity that should be present in the radiation of a random fiber laser. Indeed, it is known that other types of CW lasers, in particular Raman fiber lasers, which share with random DFB fiber lasers all key features except the mode structure of the generation spectrum, are sources of quasi-CW radiation. This means that despite a millisecond or microsecond time scale, the radiation is CW, and fast intensity fluctuations with a typical time scale inversely proportional to the spectral width exist. So a typical width of 1 nm gives a fluctuation time of about 10 ps. The existence of such fast intensity fluctuations has been experimentally demonstrated in a recent paper [113]. In this paper, the output radiation of the random DFB fiber laser was measured with the help of a real-time oscilloscope with a total bandwidth of 33 GHz (this corresponds to the typical time of 30 ps). It was found that the output radiation of the random DFB fiber laser indeed exhibits substantial fast intensity fluctuations (Fig. 19).

Figure 19



Experimentally measured intensity dynamics of random DFB fiber laser at pump power 3 W. Reprinted with permission from [113]. Copyright 2015 Optical Society of America.

Experimental measurements of real-time intensity fluctuations allows one to address one more fundamental issue—statistical properties of the radiation. Indeed, the wide generation spectrum should lead to fast intensity fluctuations if the different spectral components are generated independently and there are no (or weak) phase relations between them. If phases of different spectral components are correlated in some way, this can lead to generation of either stable or unstable pulses, and eventually lead to mode locking. It could, conversely, lead to suppression of intensity fluctuations and formation of a so-called laminar state [114] of laser generation, in contrast to turbulent generation; see, for example, recent reviews [115] and further works [116]. Phase correlations could be revealed in measurements of statistical properties of the radiation, so the temporal and statistical properties of the radiation should be studied simultaneously.

In general, statistical properties of fiber-based systems have attracted a great deal of attention that began from the famous demonstration of optical rogue waves [117]. Since then, the field has grown rapidly, and extreme events have been observed in many systems, including Raman fiber lasers [118–120] and Raman fiber amplifiers [121]. One can find an extensive review of the field in recent works [122–124]. Further, statistical properties of quasi-CW fiber lasers (to which class random DFB fiber lasers belong) have also been studied in the context of whether or not their statistics deviate from the Gaussian and what are the reasons for such deviations [125–128]. Special measures to ensure that the statistics of the output radiation of CW fiber lasers are Gaussian are required in experimental studies of wave turbulence in optics; see, for example, [115,129].

Experimental measurements of statistical properties of fiber-based sources are not easy to perform as the optical bandwidth is usually hundreds of gigahertz (total spectral width is around a few nanometer), which is much larger than the electrical bandwidth of the measurement equipment (limited to 30–60 GHz). This results in the fact that experimentally measured statistical properties are influenced by measurement procedures, which could lead to incorrect physical conclusions about the statistical properties of the signal under study. One way to overcome this problem is to pre-filter the signal to decrease its optical bandwidth down the value of a few gigahertz [119]. However, in this way, only the statistical properties of a part of the radiation is studied (at those frequencies at which the filter is located). However, it is known that the statistical properties of different

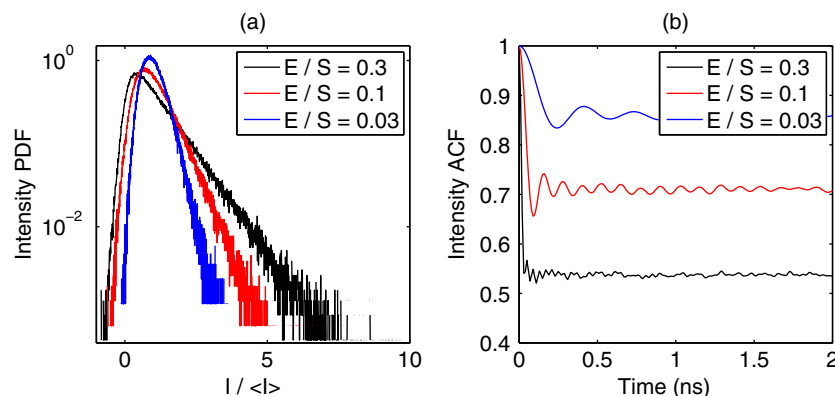
parts of the spectrum could be different, and differ, as well, from the statistical properties of the total signal, [118,119,126]. This challenge should be met while experimentally investigating statistical properties of random fiber lasers.

A general technique for how to reveal the statistical properties of the radiation in experimental conditions of limited electrical bandwidth was recently presented in [130]. Measurement with limited oscilloscope bandwidth results in cutting off frequencies higher than some maximum frequency. The influence of measurement procedure on the properties of an ideal signal with Gaussian statistics can be tracked in numerical modeling by applying a spectral filter over the radio-frequency spectrum of the modeled signal. As a result of filtering, the intensity probability density function (PDF) slope increases rapidly while bandwidth is reduced [Fig. 20(a)]. The reason for this is that events of extreme intensities are averaged out in the bandwidth limited measurements of time traces. The background level of the intensity autocorrelation function (ACF) is increased from the level of 0.5 (Gaussian statistics), while the measurement bandwidth is decreased [Fig. 20(b)]. Indeed, small values of E/S lead to substantial averaging of the fast intensity fluctuations, as seen in Fig. 20(a), which results in increasing the level of intensity ACF [Fig. 20(b)]. In the limiting case of $E/S = 0$, the intensity PDF should have the form of a δ -function centered at $I = \langle I \rangle$ as there will be no fluctuations. Consequently, the intensity ACF for such a measured signal will have a background level of 1. A similar approach was used in a recent paper to characterize statistical properties of turbulent-like fiber-optic systems [116].

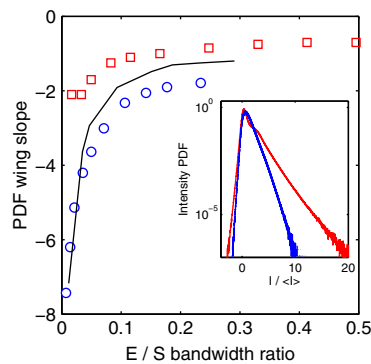
It is important that the behavior of the intensity PDF and ACF are universal if plotted over the dimensionless parameter (a ratio of electrical to optical bandwidths, E/S). The intensity PDF slope and the level of the intensity ACF function take some distinct values for each E/S ratio if the statistics of the signal under study are Gaussian. This allows directly revealing in experiments if the statistics of the studied signal are Gaussian or not.

The first experimental measurements of the statistical properties of a random DFB fiber laser using the described procedure were reported in [113]. The

Figure 20



Changes in the shape of (a) the intensity PDF and (b) intensity ACFs of the ideal signal with Gaussian statistics at different values of the electrical-to-spectral bandwidth ratio, E/S . Reprinted with permission from Ref. [130]. Copyright 2014 Optical Society of America.

Figure 21

Experimentally measured statistical properties of the random DFB fiber laser. The slope of the intensity PDF is shown: squares, at pump power 1.6 W; circles, at pump power 3 W; line, numerical prediction for a signal of Gaussian statistics. Inset: intensity probability density function at powers 1.6 and 3 W. Reprinted with permission from [113]. Copyright 2015 Optical Society of America.

measured intensity PDF has a nonexponential shape; see Fig. 21. Despite the fact that measurements were bandwidth limited (i.e., the bandwidth of the measurement equipment was smaller than the actual optical bandwidth of the signal), it was found that the radiation statistics of the studied random DFB fiber laser deviates from the Gaussian, as dependence of the PDF slope does not coincide with that predicted for Gaussian statistics [Fig. 21]. At high powers, the intensity PDF of the random DFB fiber laser is narrower than predicted for Gaussian statistics as the PDF slope has lower levels than predicted. At low power, the intensity PDF is broader than for Gaussian statistics. Note that further extensive experimental studies are required to reveal if the statistics are Gaussian or not in different configurations of random DFB fiber lasers as statistical properties could depend on the fiber parameters, laser length, etc.

4. Theoretical Description of Spectral Properties of Random Fiber Lasers

4.1. Linear Spectral Narrowing Near the Generation Threshold

4.1a. Numerical Simulation of Spectral Narrowing within the Modified Power Balance Model

Theoretical description of the spectral properties of random fiber lasers is a challenging task. In this section we review recent efforts devoted to theoretically describing the spectral properties of random fiber lasers.

Only a few works have so far been devoted to theoretical description of the spectral properties of random DFB fiber lasers. Most of these works present results of the numerical modeling of spectral performance. The simplest model of the random fiber laser is the power balance model, which describes the average power performance, such as generation threshold, output power value, generation efficiency and its optimization, and the longitudinal distribution of the power generated along the fiber length [48]. Results of the description of power

performance of random DFB fiber laser are summarized in a review [26]. To describe the spectral and temporal properties of the class of quasi-CW fiber lasers to which random DFB fiber lasers belong, NLSE-based models are usually used. Within NLSE-based models, the spectral properties of various types of quasi-CW fiber sources can be described, such as ytterbium-doped fiber lasers [131] and Raman fiber lasers [126,127]. Recently, the NLSE-based model has also been applied for description of the temporal and spectral properties of random DFB fiber lasers [44].

The nature of NLSE-based models is simultaneous taking into account all major effects in optical fibers, such as gain, loss, dispersion (including high-order dispersion coefficients), and nonlinearity. As a result, precise description of the observed properties of the radiation can be performed, but results often lack a physical understanding of concurrent processes. This is the case of random DFB fiber lasers, where, obviously, physical processes of very different natures take place at different power levels. Indeed, the generation spectrum starts to be gradually narrower while pump power increases, but then the spectral narrowing is changed to the well pronounced spectral broadening [Fig. 6(b)]. Simpler models allow distinguishing different processes and provide insight behind the different regimes of operation of random fiber lasers.

The power balance model [Eqs. (1)] is such a simple tool, as it does not take into account anything except gain and losses, i.e., dispersion and nonlinearity are not considered within this model. However, it also does not take into account any spectral properties, as the gain is spectrally independent in the power balance model. The challenge of describing the spectral properties of a random fiber laser within the modified power balance model is met in a recent paper [43]. In this paper, the power balance model is rewritten in terms of spectral power densities, instead of integral (over spectrum) powers, and the spectral dependence of the Raman gain is taken into account, as well as the spectrally dependent spontaneous Raman scattering. This allows clear description of the initial stage of the formation of the random fiber laser generation spectrum (at low pump power), i.e., to describe how the random laser comes to be different from the amplified spontaneous emission (ASE) source at low pump and generation power. This can be tracked by spectral narrowing of the generation of the random laser starting from the initial broad gain profile.

The spectral properties of radiation of a random DFB fiber laser could be taken into account by modifying the power balance model [Eqs. (1)] in the following way: spectral power densities $I_\omega = dI/d\omega$ are used instead of total powers I , the spectral dependence of the Raman gain is taken into account $g_R \rightarrow g(\omega)$, and terms corresponding to spontaneous Raman scattering are added to the equations. The resulted model reads

$$\pm \frac{dP^\pm}{dz} = -\alpha_p P^\pm - \frac{\omega_p}{\omega_s} P^\pm \left(\int g(\omega) (I_\omega^- + I_\omega^+) d\omega + 4\hbar\omega_s \right), \quad (2a)$$

$$\pm \frac{dI_\omega^\pm}{dz} = -\alpha_s I_\omega^\pm + g(\omega) (P^+ + P^-) (I_\omega^\pm + 2\hbar\omega_s) + \epsilon I_\omega^\mp. \quad (2b)$$

Here, I_ω denotes the spectral power density of the Stokes wave, $\omega_{p,s}$ are central frequencies of the pump and Stokes waves, ω is the detuning of the generation frequency from ω_s , and \hbar is the reduced Planck constant.

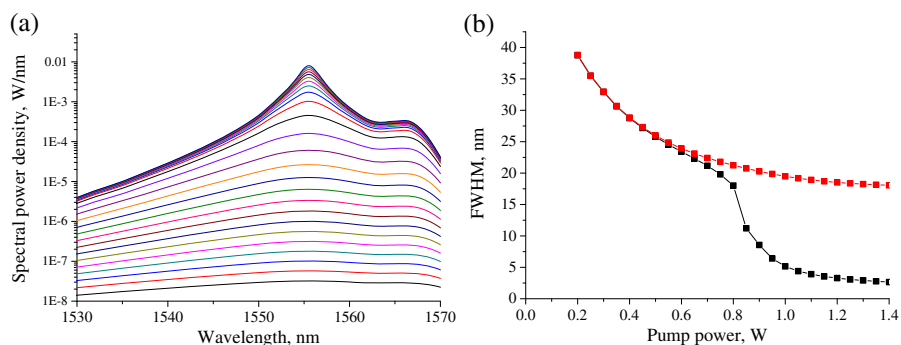
The spectrally dependent power balance equation set [Eqs. (1)] does not include any nonlinear effects, so it is capable of describing the spectral properties of the random fiber laser only on a linear stage when nonlinear effects are negligible. The influence of nonlinearity will be described further in Section 4.2.

It is assumed that the pump wave is depleted by some number of Stokes waves generated at different frequencies within the Raman gain profile, and different generation frequency components are generated independently. This means that Eq. (2b) is effectively the set of independent equations on the intensity of each generated spectral component at each frequency (the frequency discretization depends on the desired accuracy of the calculation of the optical spectrum over frequency). Note that, in the initial power balance model [Eqs. (1)], the generation wave is assumed to have a linewidth much narrower than the Raman gain bandwidth. Indeed, the generation spectrum is about 1 order of magnitude narrower (typical spectral width of the order of 1 nm) than the Raman gain spectral profile (typical spectral width of the order of 10 nm).

The power balance model does not include the Kerr nonlinear coefficient, so it cannot describe nonlinear effects such as four-wave-mixing inside the Stokes wave spectrum or cross-phase modulation between the pump and the Stokes waves. Meanwhile, it is well known that nonlinear broadening is a crucial factor in determining the spectral shape of the generation in conventional Raman fiber lasers [132–134], and spectral broadening is also observed in random fiber lasers; see Fig. 6(b). So only the region of the pump power under and near the generation threshold where nonlinearity is not important should be considered within the spectral power balance model.

Although the generation spectrum can be found by calculating the full set in Eqs. (2), the simpler approach can be implemented because generation intensities at different frequencies are coupled to the same pump wave and can be found if the pump wave longitudinal distribution $P(z)$ is known [135]. To find the pump power distribution, one can use the spectrally independent power balance model [Eqs. (1)]. Pump power distribution $P(z)$ found from Eqs. (1) can be further used in Eq. (2b) to find the generation spectrum shape, $I(\omega)$ [135]. This can be done under the assumption that the total generation power is small, and that the redistribution of the generated power over the spectrum [from single

Figure 22



(a) Spectra modeled for different pump powers. (b) Full width at half-maximum for different pump powers. Red squares indicate the model with no feedback. Reprinted with permission from Ref. [135].

frequency in Eqs. (1) to multiple frequency components in Eq. (2b)] does not change substantially the pump wave longitudinal distribution.

The results of spectral modeling for different pump powers for a single-arm laser operating at 1550 nm are shown in Fig. 22(a) (from [43]). For small pump powers, only the broadband spectrum corresponding to ASE is generated. With a pump power increase, the spectrum of the ASE gradually narrows, demonstrating the superluminescent regime. However, after a certain pump power level, the output spectrum narrows abruptly [Fig. 22(b)]. At the same time, the total generated Stokes power found as $\int I_{\omega}^{-} d\omega$ starts to grow. Thus, this is a generation threshold. Above the threshold, the generation spectrum has the form of a distinct well-pronounced single peak situated at the maximum of the Raman amplification profile [Fig. 22(a)]. While the pump power increases above the generation threshold, the spectrum becomes further narrower, in qualitative agreement with experimental observations [Fig. 6(b)]. Note the difference between the linewidth of the random fiber laser and the source of ASE (the power of the ASE source can be calculated within the same model if the backscattering coefficient, ϵ , is set to zero) [Fig. 22(b)].

Thus, a simple approach based on the modified power balance model provides insight on the initial stage of the formation of the random fiber laser's generation spectrum and qualitatively describes the spectrum narrowing above the generation threshold. In particular, one can trace how the spectrum acquires its spectral shape by starting from the initial gain spectrum, and how the power and spectral properties of a fiber laser based on random feedback are different from those of an ASE source without any feedback.

Note that a similar approach can be used for a random fiber laser based on an alternative gain mechanism. In this way, the spectrum of a hybrid EDF–Raman-gain-based random fiber laser has been numerically calculated in a qualitative way in [93]. To calculate the spectrum of such a laser, the power balance model for Raman gain should be combined with a model of EDF gain based on the propagation and rate equations of a homogeneous, two-level active medium [136].

4.1b. Spectral Narrowing within the Modified Schawlow–Townes Approach

In general, it is common knowledge in laser physics that the lasing spectrum becomes narrower while the pump power increases inversely proportional to the power [137]. In their seminal paper, Schawlow and Townes used simple considerations that, in fact, are very similar to those used in the modified power balance model. For a random fiber laser, the modified Schawlow–Townes approach could also be used to describe the spectral narrowing of the generated radiation near the generation threshold of a random fiber laser. Further, we follow the description from [138].

One can substantially simplify the spectral power balance model [Eq. (2b)], and gain analytical insight into the processes of spectral narrowing near the generation threshold. Indeed, just below and near the generation threshold, the generation power is very low, so one could omit the influence of the generation wave on pump wave depletion. In this case, the longitudinal distribution of the pump wave takes the simple exponential form defined by the linear losses for the pump wave: $P(z) = P_0 \exp(-\alpha_p z)$. The following derivation is applied

for a random laser configuration with a pump wave propagating toward an output (see [26] for description of different laser schemes), and for the case $\alpha_p L \ll 1$, that means uniform distribution of pump power $P(z) \sim P(z=0) = P$. Here L is the laser length.

For the strong generation wave propagating toward the output, the corresponding power balance equation takes a simple form if one neglects Rayleigh back-scattering from the backward propagating generation wave ϵI_ω^- , as it has a small impact because of small intensity of the backward generation wave I_ω^- :

$$\frac{dI_\omega^+}{dz} = (g(\omega)P - \alpha_s)I_\omega^+ + 2g(\omega)P\hbar\omega_s. \quad (3)$$

Here, ω_s is carrier angular frequency. In this assumption, the forward propagating generation wave exponentially grows: $I_\omega^+(z) = I_\omega^{\text{out}} e^{(g(\omega)P - \alpha_s)(z-L)}$.

The power balance equation for the backward wave I_ω^- propagating from the output has the form

$$-\frac{dI_\omega^-}{dz} = (g(\omega)P - \alpha_s)I_\omega^- + 2g(\omega)\hbar\omega_s + \epsilon I_\omega^+. \quad (4)$$

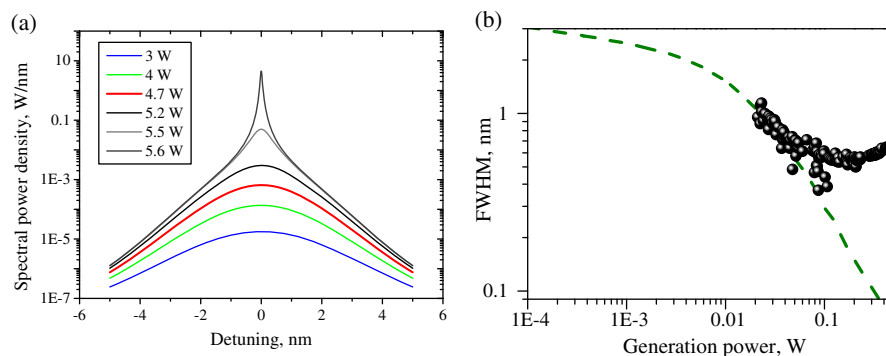
We remind the reader that frequency ω is the frequency detuning from the center of the gain profile.

With appropriate boundary conditions, $I_\omega^-(L) = I_\omega^+(L)$, for a backward pumping scheme, (see [138]) the output generation spectrum of the random distributed fiber laser near generation threshold is derived:

$$I_\omega^{\text{out}} = 4\hbar\omega_s \frac{g(\omega)P(e^{(g(\omega)P - \alpha_s)L} - 1)}{g(\omega)P - \alpha_s} \frac{e^{(g(\omega)P - \alpha_s)L} + 1}{1 - \frac{\epsilon(e^{2(g(\omega)P - \alpha_s)L} - 1)}{2(g(\omega)P - \alpha_s)}}. \quad (5)$$

Taking a specific shape of the Raman gain spectral profile, one can calculate from Eq. (5) the resulting shape of the random fiber laser's generation spectrum. Results of calculation in the case of a Raman gain profile presented in the form of a Lorentzian function with width Γ_R , i.e., $g(\Delta\omega) = g_R/(1 + (\Delta\omega^2/\Gamma_R^2))$, are shown in Fig. 23(a). The spectrum becomes gradually narrower while the pump power increases. The spectral narrowing law is different well below the

Figure 23



(a) Wave spectrum at different pump power level. (b) Spectral full width at half-maximum. The data are numerically calculated from Eq. (5). Black circles are experimental data [138].

generation threshold and above the generation threshold [Fig. 23(b)]. Above the threshold, the spectrum becomes narrower in a manner that is inversely proportional to the generation power, similar to the Schawlow–Townes law [137]. In this way, the approach of Schawlow and Townes is extended to the case of the random fiber laser. The numeric results were verified with experimental data [Fig. 23(b)] [138].

4.2. Nonlinear Kinetic Spectral Broadening

4.2a. Principles of the Wave Kinetic Approach in Application for Random Fiber Lasers

Previously, we have described the ultimate power properties of random fiber lasers within the simplest power balance equation set [Eqs. (1)], which does not take into account nonlinearity or spectral properties. Then, in the previous section, the narrowing of the generation spectrum of the random DFB fiber laser is shown within the linear spectrally dependent model. However, at high power, the nonlinearity starts to play an important role and the spectrum exhibits broadening [Fig. 6(b)]. Here we provide a description of the spectral properties of the random fiber laser within nonlinear theory.

Very recently, in [138], the spectrum of the random fiber laser was described by nonlinear kinetic theory derived within a general approach of active cyclic wave kinetics. Here we will overview this approach and highlight the most important steps relative to the description of the random fiber laser’s generation spectrum.

It is well established in optics that the system properties can be described in a dynamical way by means of the NLSE. The NLSE describes the evolution of the envelope of the generation electromagnetic field, ψ , over coordinate z within the fiber, at $0 < z < L$. Here L denotes the length of the random fiber laser. The equation for the generation wave propagating in the fiber to the right is

$$i(\partial_z - \hat{g}/2)\psi = \frac{\beta}{2}\partial_t^2\psi + \gamma\psi|\psi|^2, \quad (6)$$

in which t stands for time, γ is the Kerr nonlinear coefficient, and β is the quadratic dispersion coefficient. The noise is neglected. The effective gain operator \hat{g} is defined by the balance of gain and optical losses and is frequency dependent. The spectral dependence of the gain coefficient is approximated by parabolic law for simplicity:

$$\hat{g}(\omega) = g_R P(z) - \alpha - aP(z)\omega^2. \quad (7)$$

Here g_R is the Raman gain coefficient, $P(z)$ is the power of the pumping wave, α is the linear losses in the fiber on the generation wavelength, and a defines gain spectral shape.

It has been recently shown that the generation properties of random DFB fiber lasers can be numerically modeled within a NLSE-based approach [44]. However, it is difficult to gain analytical insight from the NLSE about the generation spectrum shape and functional dependence of the spectral width on parameters of the random laser. An analytical approach is highly desirable. The random fiber laser belongs to the class of optical systems for which the spectral properties are defined by a large ensemble of nonlinearly interacting light waves. Such systems are natural objects not for dynamic description within

the NLSE, but for a statistical description. The statistical wave kinetic approach (known in some contexts as wave turbulence [139]) is used in a range of physical applications varying from Bose–Einstein condensates to astrophysics [140]. Traditional wave kinetics describes the slow evolution of systems with many degrees of freedom to equilibrium via numerous weakly nonlinear interactions. In its classical form, wave kinetics has recently been successfully applied to conservative nonlinear optical systems; see a recent review in [115]. The wave kinetic approach could provide a straightforward description of the spectrum of the optical system, as the optical spectrum I_ω is in its essence the correlation function directly described by the wave kinetic equation.

However, random fiber lasers cannot be directly described within the wave kinetic approach. Indeed, there is homogeneous dissipation and amplification over the fiber length, i.e., nonhomogeneity over the evolution coordinate (in terms of the wave kinetic approach). A classical wave kinetic description of such dissipative (active) systems with nonhomogeneous evolution is impossible. A conceptually new formalism for description of such systems—wave kinetics of active cyclic systems—is introduced in [138].

In active cyclic systems, as in any laser, including random fiber lasers, the energy pumping (through optical gain) and energy dumping (through optical losses, in particular on the output mirror of the laser cavity) act in a periodic way as the light is trapped within the laser cavity making the round-trip there. The resulting dynamics of the optical spectrum has a cycling nature and exhibits double-scale evolution. Indeed, the generation spectrum could be strongly reshaped during propagation over the fiber (i.e., within each cycle) because of optical gain and optical losses. At the same time, on another time scale—cavity round-trip time—the generation spectrum is subject to only incremental changes (from one round trip to another round trip), if the laser operates in the stationary regime (i.e., the initial process of radiation onset after switching the pump on has settled down). Classical wave kinetics cannot deal with systems that include double-scale evolution, i.e., the generation spectrum of lasers cannot be described in a kinetic way. However, paper [138] meets this challenge and presents an approach to the wave kinetics of active cyclic systems that allows description of the spectrum of lasers, including random fiber lasers. To do that, the so-called local wave kinetic equation should be derived. This equation governs the evolution of the generation spectrum and its solution provides an equilibrium shape of the spectrum.

The special case of a short random fiber laser with backward pumping is considered in [138]. This means that the power of the generation wave increases rapidly in the small region near the output fiber end; see [26]. Thus, backscattering is most effective only near the fiber end as the backscattering intensity is proportional to the intensity of the generated wave. That is why the reflection could be treated as point-based reflection, and boundary conditions that couple the generation wave ψ_+ , propagating to the right, with generation wave ψ_- , propagating to the left, have the form of $\psi_+ = \hat{R}(\omega)\psi_-$.

The essence of the wave kinetic approach is to describe not the evolution of the complex wave amplitude ψ as in the dynamical NLSE model, but to describe the evolution of a statistical quantity, i.e., of the correlation function defined as

$$\langle \psi(z, t_1 + t)\psi(z, t_1) \rangle = \int \frac{d\omega}{2\pi} \exp(-i\omega t) I(z, \omega), \quad (8)$$

where angle brackets denote averaging over z larger than the dispersion length $L_d = 1/(\beta\Delta^2)$, where Δ is the characteristic width of the wave spectrum.

Note that the optical spectrum directly measured in an experiment is the same Fourier transform of the correlation function, i.e., the wave kinetic equation directly governs the evolution of the optical spectrum over the fiber length and defines the generation spectrum shape.

The boundary conditions for the optical spectrum can be rewritten as

$$I(0, \omega) = |R(\omega)|^2 I(L, \omega) \quad (9)$$

for the generation wave propagating to the right. This condition relates values of the correlation function I taken at different ends of the fiber.

As a next step one can derive the wave kinetic equation on correlation function I_ω under the assumption that there are numerous nonlinearly interacting waves with random phases. Extensive technical details can be found in [138,141]. Here we provide key assumptions under which analytical insight into the generation spectrum of a random fiber laser can be gained.

It is assumed that the generation spectrum of a random laser should be narrower than the gain profile, i.e., $aP\Delta^2 \ll g_0$, where Δ is spectral width.

It is important that Gaussian statistics of the fluctuations of the field ψ are assumed. As it has been shown in Section 3.3, the statistical properties of real random DFB fiber lasers could deviate from Gaussian. This could lead to deviations of theoretically predicted spectral properties from experimentally observed in such systems.

Under the listed assumptions, the following generalized local wave kinetic equation describing the evolution of the generation spectrum of a random fiber laser can be derived:

$$\begin{aligned} & (\partial_z - g_0 + aP\omega^2)I_\omega \\ &= 4\gamma^2 \int \frac{d\omega_1 d\omega_2 d\omega_3}{(2\pi)^2} \delta(\omega + \omega_1 - \omega_2 - \omega_3) \\ & \quad \times \frac{g_0}{g_0^2 + \left[\frac{\beta}{2}(\omega^2 + \omega_1^2 - \omega_2^2 - \omega_3^2)\right]^2} [I_\omega I_2 I_3 + I_1 I_2 I_3 - I_\omega I_1 I_2 - I_\omega I_1 I_3]. \quad (10) \end{aligned}$$

Here, $I_\omega = I(z, \omega)$, $I_i = I(z, \omega_i)$. We remind the reader that ω is frequency detuning from the central wavelength ω_s .

In Eq. (10), the left-hand side term describes a linear process of spectral narrowing because of the wavelength dependence of $\hat{g}(\omega)$. The right-hand term is the nonlinear interaction between different spectral components I_ω, I_1, I_2, I_3 . Note that integration of Eq. (10) over frequency ω for obtaining total power $I = \int I_\omega d\omega$ results in vanishing of the right-hand side term, as it does not alter the total power but redistributes the power among different wavelengths.

Note that a process of gain saturation should be included in the model to find solution I_ω above the threshold. In a Raman fiber laser, gain saturates above threshold because of pump $P(z)$ depletion and because of spectral broadening, which decreases an effective gain g_{eff} averaged over the generation spectrum. Although one approach is to consider evolution of the pump wave and introduce

the g_{eff} into the model, these effects can also be taken into account by involving additional single parameter $\eta(P)$, which defines the difference between undepleted integral gain $\exp(\int_0^L dz g_0(P))$ (which is equal to losses at the threshold) and the actual one:

$$|R(\omega)|^2 \exp\left(\int_0^L dz g_0(P)\right) = 1 + \eta(P). \quad (11)$$

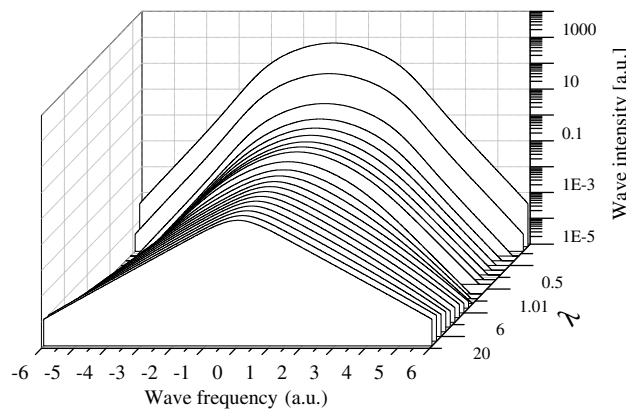
Within this notation and in the case of small nonlinearity $\gamma I \ll \beta \Delta^2$, the wave kinetic equation describing the shape of the random fiber laser's generation spectrum takes the form

$$\begin{aligned} & (\eta - \mathcal{A}\omega^2)I_\omega + 2\gamma^2 \int \frac{d\omega_1 d\omega_2 d\omega_3}{(2\pi)^2} \delta(\omega + \omega_1 - \omega_2 - \omega_3) \\ & \times \frac{1}{g_0^2 + \left[\frac{\beta}{2}(\omega^2 + \omega_1^2 - \omega_2^2 - \omega_3^2)\right]^2} [I_\omega I_2 I_3 + I_1 I_2 I_3 - I_\omega I_1 I_2 - I_\omega I_1 I_3] = 0, \end{aligned} \quad (12)$$

in which all functions are taken at $z = L$ and $\mathcal{A} = \int_0^L dz aP$. Integrating Eq. (12) over ω gives simple relation $\mathcal{A}\Delta^2 = \eta$. From the other hand, total output power I can be also determined through η . This makes possible defining saturation parameter $\eta(P)$ from experiment.

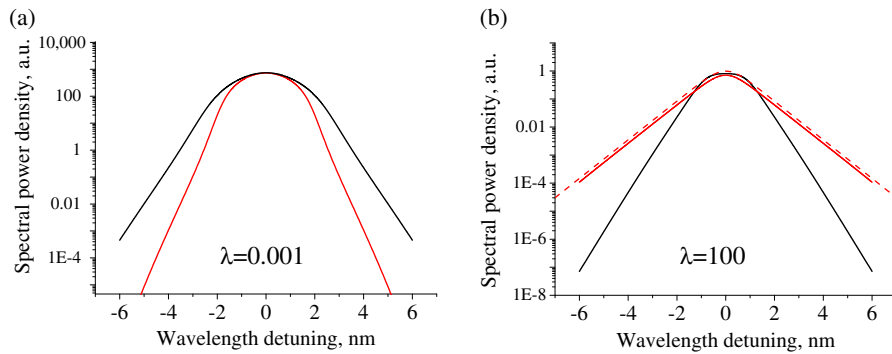
Nondimensionalization of Eq. (12) gives only a parameter of the ratio between gain and dispersion, $\lambda = 2g_0P/\beta\Delta^2$. Thus, a stationary spectrum shape of the random DFB fiber laser depends only on the value of parameter λ (Fig. 24). At small λ , the shape of most of the spectrum (down to the value of -20 dB relative to the spectral power density in the maximum) is close to Gaussian shape, $\exp(-\omega^2)$ [Fig. 25(a)]. However, the far spectral tails at large detunings from the spectrum center have different asymptotics—they are exponential, $\exp(-\Theta|\omega|)$. Note that the case of small λ does not directly correspond to the case of small total gain (i.e., small pump power), as parameter λ comprises the spectral width Δ in its denominator. It should also be noted that at small gain (power), the spectrum shape is strongly influenced by processes of linear kinetic

Figure 24



Shape of the random DFB fiber laser generation spectrum numerically calculated for different ratios between gain and dispersion [138].

Figure 25



Dependence of the spectrum of the random DFB fiber laser on spectral shape of the Raman gain. Red, Raman gain $g(\omega) \sim (1 - \omega^2)$; black, $g(\omega) \sim (1 - \omega^4)$. (a) Large dispersion limit. (b) Small dispersion limit. Dashed line, hyperbolic secant law.

spectral narrowing; see Section 4.1. So proper experimental observations of an almost Gaussian spectrum should be done in a random fiber laser made of a fiber with large dispersion coefficient β under high pump power.

At large values of parameter λ , which corresponds to the limiting case of the small dispersion, $\lambda \rightarrow \infty$, the generation spectrum has a very different spectral shape. Indeed, in this case, one can analytically solve the wave kinetic equation [Eq. (12)] and find that the generation spectrum has the shape of a hyperbolic secant, $\text{sech}(\omega)$; see [138] for technical details.

The limiting case of the hyperbolic secant shape is valid only within the approximation of the parabolic Raman gain [Fig. 25(b)]. In the case of another spectral shape of the gain profile, the resulting spectrum shape of the generation spectrum will be different. However, in the limit of large dispersion, the shape of the spectral top does not depend on the shape of the gain profile: the top of the spectrum always has a parabolic shape (but of different width) [Fig. 25(a)]. Note that the spectral wings could have different slopes in the case of different gain profiles.

It should be noted that a similar hyperbolic secant spectrum shape was experimentally observed and theoretically introduced in a phenomenological way in the limiting case of dispersion much larger than nonlinearity for a conventional Raman fiber laser with a cavity based on point-like mirrors [132]. The fact that the hyperbolic secant spectrum shape of a laser with conventional cavity design [132] coincides with the spectrum shape derived for a very different system (a random fiber laser with no cavity of fixed length) is intriguing and should be further investigated.

4.2b. Experimental Verification of Nonlinear Kinetic Theory Predictions

To experimentally check the predictions of the nonlinear kinetic theory of spectral broadening and linear kinetic theory of spectral narrowing, a specific experimental setup was designed in [138]. The random DFB fiber laser is designed to have a short length of only 850 m. Phosphosilicate fiber was used because it has a single Raman gain peak with a spectral shape close to parabolic (of full width

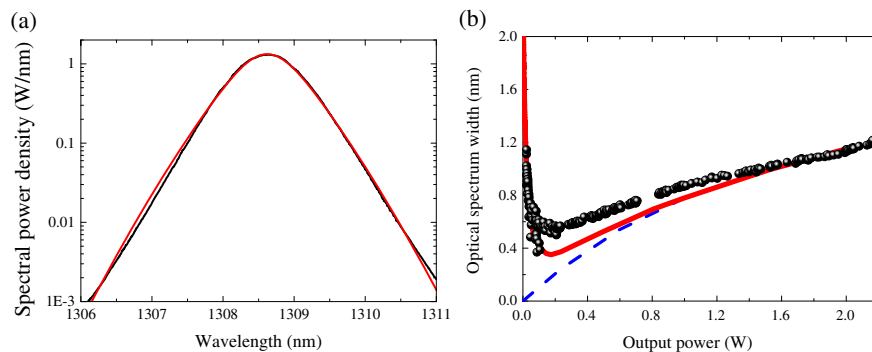
at half-maximum of about 8 nm). Note that because of the short laser length, the generation wave's intensity increases almost exponentially toward the fiber length, so the main contribution to the backscattered wave occurs near the fiber end. An important assumption of nonlinear kinetic theory, that the feedback is provided by an effective point-based reflector, is fulfilled in experimental conditions of a short random fiber laser.

To get a theoretical prediction of the generated spectrum shape and width from the nonlinear kinetic theory, one should define all parameters used in the theoretical description, namely, the shape of the gain profile, the dispersion coefficient, the nonlinear coefficient and, finally, the dependence of parameter η over power. To find experimentally the dependence $\eta(P)$ we use the experimentally measured generated power dependence over the pump power, $I(P)$. The wave kinetic equation [Eq. (12)] is numerically solved by an iterative procedure: the numerical value of the generation power I is calculated at different values of η at every fixed pump power value P ; the value of η is varied in order to achieve coincidence of calculated and measured values of generated power I . In this way, the dependence η is found from experimental data. This dependence is further used in calculations of the generated spectrum, $I(\omega)$, and its width over the pump power, $\Delta(P)$.

High above the generation threshold, the spectral shapes measured and calculated within the nonlinear kinetic theory agree well [Fig. 26(a)]. The description of the spectral broadening law is good, as well, at high power [Fig. 26(b), blue dashed line]. However, one should take into account both nonlinear spectral broadening and linear spectral narrowing. The sum of linear and nonlinear terms describes well the experimentally measured laser spectrum width in the entire power range [Fig. 26(b), red line].

Thus, the spectrum of the random fiber laser can be quantitatively described within the nonlinear kinetic theory that takes into account the nonlinear interaction between different spectral components generated in a random fiber laser.

Figure 26



Predictions for the spectrum shape and spectral width within nonlinear kinetic theory and its verification in experiment. (a) Experimentally measured (black) and theoretically predicted (red) optical spectrum at power 1.5 W. (b) Spectrum width as a function of laser output power in theory and experiment. Experimental data are shown by black circles. The prediction for spectrum broadening from nonlinear kinetic theory is shown by the blue dashed line. The red line is a sum of nonlinear and linear contributions [138].

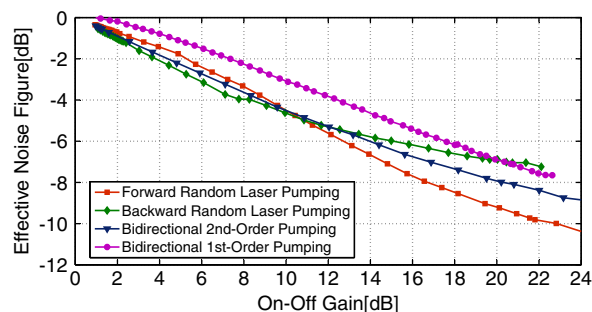
5. Applications

5.1. Random Fiber Laser for Telecommunication Applications

Random lasing can be realized in a long-distance fiber span, making it intrinsically suitable for distributed Raman amplification. Apart from advantages such as good stability and simple technical design, random-fiber-laser-based distributed Raman amplification with forward pumping possesses a lower effective noise figure compared to conventional bidirectional Raman amplification. In [142], the random fiber laser is used as a pump source in a forward-pumped distributed amplifier, which results in larger averaged gain and gain fluctuations. The effective noise figure of the forward-pumped configurations is lower than that for the bidirectional first-order pumping by ~ 2.3 dB, and lower than that of bidirectional second-order pumping by ~ 1.3 dB at transparency transmission [Fig. 27]. The unique feature of random lasing amplification has provided a new approach to enhance the performance of long-distance distributed fiber sensing, and it can also be directly implemented in long-haul optical communication systems.

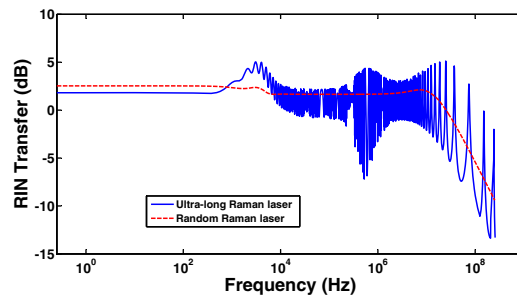
One of the main drawbacks in telecommunication distributed Raman amplifiers is the relative intensity noise (RIN) transfer, as it results in additional noise arising at signal wavelength. For possible telecom applications of random fiber lasers, a numerical study of the RIN transfer function in a forward-pumped random fiber laser was performed in [143]. To do this, the power balance model in Eqs. (1) is expanded with equations for the spectral density of the noise intensity for the pump and the Stokes waves. The RIN transfer function was calculated for different pump powers and fiber lengths. It was shown that the noise transfer decreases while the random laser cavity length or the pump power increases. The authors compared RIN transfer properties of a 100 km long random fiber laser with those for a 100 km long Raman fiber laser with a conventional fiber Bragg grating (FBG)-based cavity (Fig. 28). The averaged level of the RIN transfer function was found to be similar in the two lasers. However, in the case of the modeless random fiber laser, there are no oscillations in the noise transfer function. Note that, in a conventional Raman fiber laser, the frequency noise originates not only from the beating of the distinct longitudinal modes of the

Figure 27



Effective noise figure versus ratio of averaged power for a distributed Raman amplifier based on a random fiber laser in different pumping configurations. Reprinted with permission from Ref. [142]. Copyright 2013 Optical Society of America.

Figure 28



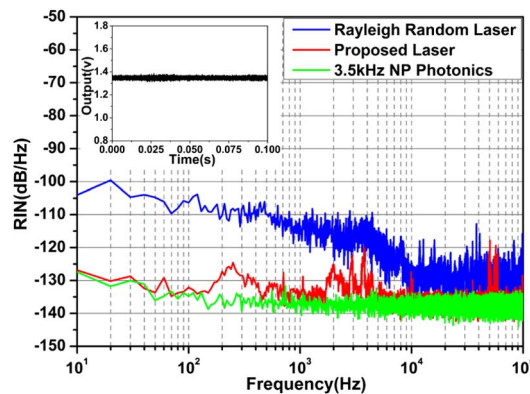
RIN transfer function in a random fiber laser (red curve) compared with those calculated for a Raman fiber laser of conventional cavity design (blue curve). Reprinted with permission from Ref. [143]. Copyright 2012 Optical Society of America.

laser cavity, but also from the pump-to-Stokes wave noise transfer [144]. The dumping of the oscillations in a random fiber laser could play a positive role in applications of random fiber lasers for distributed amplification.

Quite opposite from intuitive expectations, random fiber lasers can have noise performances that are, in some cases, superior to commercially available cavity-based solutions. Saxena *et al.* [145] recently showed that Rayleigh feedback actually suppresses noise at higher frequencies.

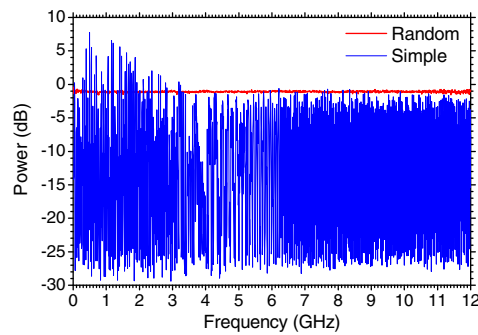
This was attributed to the fact that the frequency noise spectrum density arising out of multiple Rayleigh reflections was, in fact, a Lorentzian, which overlaps the original frequency noise of the cavity. A similar improvement in noise performance was also noted in a bidirectionally pumped Brillouin random laser [76] and in a tunable ring fiber laser based on a random fiber Bragg grating [146], as shown in Fig. 29. The realization of such low-noise narrow-linewidth sources utilizing such simple principles indeed is a promising aspect for a broad range of sensing and interferometric applications.

Figure 29



RIN level in different types of fiber lasers. The ring fiber laser incorporating a 10 cm long random fiber Bragg grating (red curve) compared with those of a single-frequency laser (green curve). Reprinted with permission from Ref. [146]. Copyright 2014 Optical Society of America.

Figure 30



Frequency response of the internally modulated random DFB fiber laser (red curve) in a comparison of the frequency response of the modulated conventional Raman fiber laser (blue curve). Reprinted with permission from Ref. [106]. Copyright 2013 Optical Society of America.

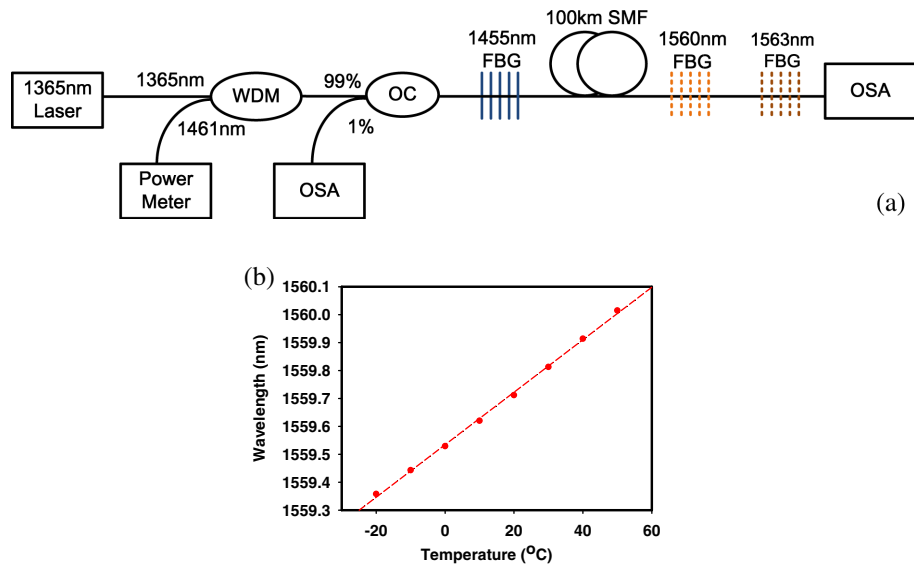
Internally modulated random fiber lasers have a response function quite different from those of lasers based on a conventional cavity. In conventional internally modulated Raman fiber lasers, the length of the laser cavity distorts the analog internal modulation and determines the repetition rate of generated pulses. In random fiber lasers, the feedback does not correspond to a fixed length, so there is no distortion of the modulating frequency or self-mode-locking effects [106]. The flat frequency behavior of the proposed random mirror laser is remarkable in comparison to the periodic frequency response of the linear cavity (Fig. 30). An internally modulated random fiber laser could be applied in time division fiber optic sensor multiplexing systems as a source for interrogating a sensor array.

5.2. Random Fiber Laser as a Remote Point-Based Sensing System

The generation spectrum of random DFB fiber lasers based on Raman gain is broad and stable over environmental conditions [147]. So, to make a random fiber laser that operates as a sensing system, one has to introduce some additional elements in the laser design. Indeed, as we have seen in Section 3.1, the spectrum of a random fiber laser follows the spectral position and width of an additional point-based spectral element. If the spectral properties of a point-based reflector (such as a FBG) are subject to change under environmental conditions, the generation spectrum of the random fiber laser will also be changed. In this way, the random fiber laser can act as a sensing system.

This concept has been implemented in [147]. In that paper, random lasing is achieved in a 100 km long fiber span via random DFB and reflection from the FBG. Two different configurations were implemented: first- and second-order lasing [Fig. 31(a)]. For the first-order regime, the laser is pumped by a 1365 nm source and a FBG sensor corresponding to the first-order Stokes wavelength (1455 nm) is placed at the other end of the fiber span. For the second-order regime, a 1455 nm FBG point mirror is placed at the pump side to facilitate 1455 nm lasing, while a 1560 nm FBG sensor is placed at the far end of the fiber span. Temperature sensing was performed via measuring the temperature-dependent wavelength shift of the random fiber laser generation spectrum

Figure 31



Point-based temperature sensing system based on a random fiber laser. (a) Experimental setup. (b) Temperature sensitivity. Reprinted with permission from Ref. [147]. Copyright 2012 Optical Society of America.

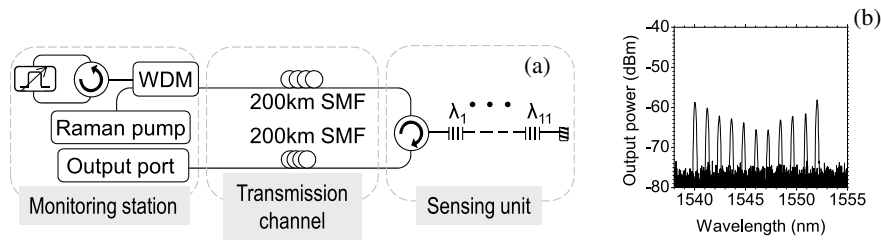
measured at the pump side of the laser. The typical dependence of the generation wavelength on the FBG temperature is shown in Fig. 31(b).

This scheme is attractive for practical applications for several reasons. First of all, the sensing element is purely passive and far (beyond 100 km) from the interrogator, which is a mandatory requirement for sensing in harsh environments. The next point is that the retrieval of the sensing parameter is in the wavelength domain, which depends only on the Bragg wavelength of the FBG sensor, making the system robust against degradation of the pump source or fiber span. Finally, the OSNR of the lasing line can be as high as 20 and 35 dB for the first order and the second order, respectively, suggesting that the ultimate limit of such a sensing system can be significantly beyond 100 km. Therefore, the thermal stability and the ultralong signal delivery make the RDFBL an accurate remote sensing system.

A 200 km long point-sensing system has been realized within an approach similar to that shown in Fig. 32. The OSNR values for the reflected sensing signals vary from 17 dB in the best case to 10 dB in the worst case, because of the longer length of the system [148]. The demonstrated temperature sensitivity amounts to 11.3 pm/°C. Note that the system is multiwavelength, providing the possibility of simultaneous sensing of the temperature at up to 11 points. This number can be further increased, as a random fiber laser based on a set of 22 FBGs and operated on up to 22 different wavelengths was demonstrated [55].

The types of point-based reflectors used in random-fiber-laser-based sensor systems can vary. In [149], a suspended-core Fabry–Perot interferometer is used at the pump side of the random fiber laser [Fig. 33(a)]. Similar to an FBG, this element acts as both the reflective mirror of the laser and the sensing element for temperature sensing. Together with the broadband mirror created by multiple Rayleigh scattering along the 2.4 km DCF, the Fabry–Perot interferometer results in multiwavelength random lasing. The resulting temperature sensitivity

Figure 32

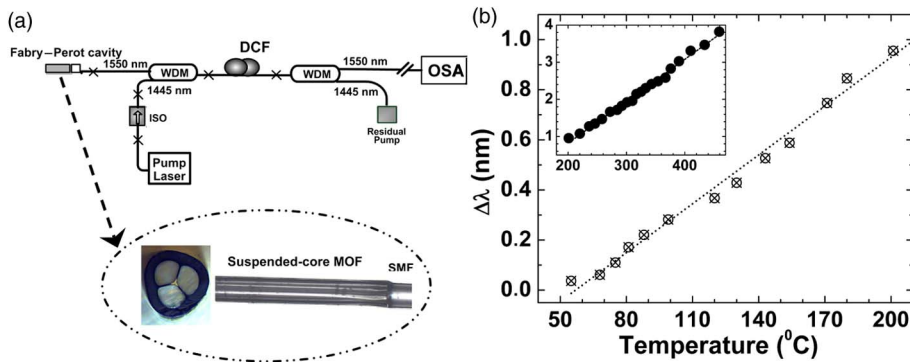


200 km long multipoint temperature sensor system based on a random fiber laser. (a) Experimental setup. (b) Generation spectrum of the multiwavelength signal used for temperature sensing. Copyright 2013 IEEE. Reprinted, with permission, from Fernandez-Vallejo, IEEE Photon. Technol. Lett. **25**, 1362–1364 (2013) [148].

is ~ 6 pm/ $^{\circ}\text{C}$, in a 50–200 $^{\circ}\text{C}$ temperature range [Fig. 33(b)]. Similarly, if the Fabry–Perot interferometer is replaced by a highly birefringent photonic-crystal-fiber-based loop mirror, the random fiber laser can also be used for temperature or strain sensing [59].

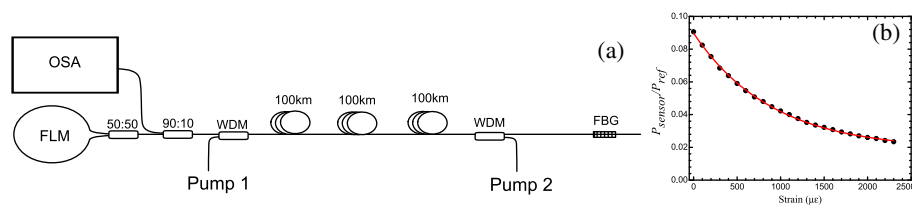
The concept of temperature-insensitive strain measurement via generation in a random fiber laser was proposed in [150]. In that work, two FBGs were used as sensing elements in the configuration of an 11 km long random fiber laser. The laser consists of 1 km of DCF and 10 km of conventional telecom fiber. The generation wavelength of the random fiber laser is defined by the spectral response of the FBGs, which, in turn, could be tuned by temperature or strain variations. It should be noted that a 10 km section of SMF between the DCF and the FBGs can be considered as only a transmission medium, because no pump light is present in it and its integral Rayleigh scattering is 3 orders of magnitude smaller than the reflectivity of any FBG used. It has been demonstrated that a random fiber laser operates at two different wavelengths simultaneously, which makes possible and efficient four-wave mixing between these two lines in a long fiber because of its low dispersion. As a result, the random fiber laser

Figure 33



Random-fiber-laser-based sensor system with a Fabry–Perot interferometer as the sensing element. (a) Experimental setup. (b) Sensitivity of the generation wavelength over the temperature. Reprinted with permission from Martins *et al.*, Appl. Phys. B **105**, 957–960 (2011) [150]. Copyright 2011 AIP Publishing LLC.

Figure 34



300 km long strain sensor system based on coupled random fiber lasers: (a) experimental setup and (b) results of strain measurement. Reprinted with permission from Ref. [151]. Copyright 2011 Optical Society of America.

could be operated as a temperature-insensitive strain sensor, as both sensors have the same sensitivity to temperature but only one of the FBGs is sensitive to strain. The demonstrated strain sensitivity is around $2 \text{ pm}/\mu\epsilon$.

The distance at which the strain can be measured remotely could be increased. For example, an ultralong remote point-sensing system has been demonstrated as two forward-pumped random fiber lasers are connected together [151]: a fiber loop mirror and a FBG are placed at different ends of the 300 km fiber span. The system, if pumped by high-power 1455 nm Raman pump sources, lases at around 1550 nm [Fig. 34(a)].

In this scheme, one random fiber laser operates via broadband reflection from the fiber loop mirror and the random DFB from the fiber span, while another random fiber laser is formed by the feedback from the FBG and the random feedback from the fiber span. Note that there is no lasing defined by light reflection either from the loop mirror and the FBG forming the ultralong cavity. Indeed, the system length—300 km—is longer than the limit of the length for a linear-cavity Raman fiber laser at which the feedback between two point-based mirrors can be established and can define the lasing properties. This limit was found to be about 270 km [152]. If the length is greater than 270 km, the laser operates via random DFB only, and point-based reflectors placed at different ends of fiber the span cannot form the cavity.

In the 300 km long dual-wavelength random fiber laser, lasing from a FBG-based laser was used for strain sensing, while lasing via a fiber loop mirror was used as a reference signal. By measuring the output power ratio between the two laser lines, the applied strain on the FBG can be retrieved with sensitivity up to $9.0 \cdot 10^{-6} \mu\epsilon^{-1}$ [Fig. 34(b)]. Using of the random fiber laser provides four-fold enhancement in sensitivity comparing with a 230 km long FBG sensor system based on a high-speed swept-wavelength light source [153]. Although an active device is needed near the sensing head in the case of a random fiber laser, limiting its sensing applications, this work is a clear illustration that a slight perturbation on the fiber end of a long random fiber laser makes noticeable changes in the generation spectrum of the laser.

To date, all random-fiber-laser-based sensing systems incorporate some point-reflector-based sensing elements. There has so far been no work about a purely distributed random fiber laser as a sensing system. Nevertheless, it is already interesting to see that in random fiber lasers of different pump and cavity configurations, sensing performance can be vastly tailored.

5.3. Random Fiber Laser for Applications in Distributed Sensing

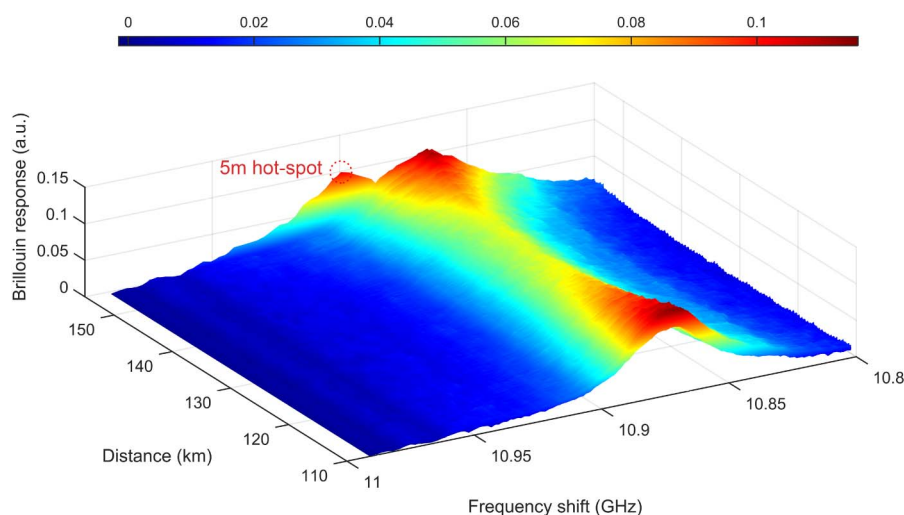
The concept of random-fiber-laser-based distributed amplification can be combined with the concept of distributed sensing. As a proof-of-principle experiment, a Brillouin optical time-domain analysis (BOTDA) reflectometer incorporating a random fiber laser to increase the SNR was demonstrated in [154]. This system allows continuous sensing of temperature over a 122 km fiber span with ± 2 m spatial resolution and $\pm 14^\circ\text{C}$ temperature accuracy.

Further extension of sensing distance is mainly restricted by the relatively high pump power requirement (multiple-watt level typically) and detrimental nonlinear effects. To address this issue, a hybrid pumping configuration was proposed in [69]. The system is pumped by a low-noise laser-diode-based Raman fiber laser that acts as a first-order Raman pump for the random fiber laser. This allows increasing the OSNR value on the far end of the sensing system and reaching a sensing length of 154.4 km with 5 m spatial resolution and $\pm 1.4^\circ\text{C}$ temperature accuracy [Fig. 35]. The demonstrated Brillouin optical time-domain reflectometer has the longest repeaterless sensing range reported to date.

Another configuration implementing only one pump source is described in [155]. In this system, a ring configuration is used to extend the system length: sensing over 142.2 km of fiber with 5 m spatial resolution and $\pm 1.5^\circ\text{C}$ temperature accuracy was achieved. Although the sensing distance is 12 km less than that in paper [69], only one pump source is needed in [155].

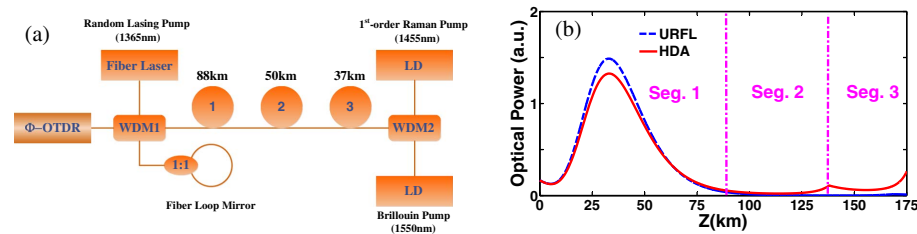
A random-fiber-laser-based distributed amplifier can also be incorporated into other types of distributed optical fiber sensing systems for extension of sensing distance. As an impressive demonstration, phase-sensitive optical time-domain reflectometry (Φ -OTDR) with a 175 km sensing range and ± 12.5 m spatial resolution was demonstrated in [156]. In that work the authors utilize the

Figure 35



Brillouin optical time-domain reflectometry based on a random fiber laser. The temperature distribution is measured over a 150 km fiber span. The temperature value is color coded. Reprinted with permission from Ref. [69]. Copyright 2013 Optical Society of America.

Figure 36



175 km Φ -OTDR with hybrid distributed amplification: (a) experimental setup and (b) calculated Rayleigh backscattering signal in the case of an ultralong Raman fiber laser (URFL) configuration and the configuration based on a random fiber laser with hybrid distributed amplification (HDA). Reprinted with permission from Ref. [156]. Copyright 2014 Optical Society of America.

combination of a copumped random-fiber-laser-based distributed amplifier with counterpumped first-order Raman amplification and Brillouin amplification [Fig. 36(a)]. The 1455 nm random lasing generated under the forward pumping provides distributed amplification for the probe pulse all the way along the first 88 km fiber span (Segment 1), making the probe pulse efficiently amplified via the Brillouin gain in the range from 88 to 138 km (Segment 2). First-order Raman amplification takes over the signal boosting in Segment 3 of 37 km length. In such configuration, the longest repeaterless distributed phase-sensitive time-domain reflectometer was demonstrated [Fig. 36(b)].

For the forward-pumped random-fiber-laser-based distributed sensing systems, the sensing distance and OSNR could be further improved by using high-order random fiber lasers [70]. Indeed, the position of the maximum longitudinal distribution in the random fiber laser shifts toward longer distances for the high-order Stokes waves [26]. Also, with the forward-pumped random-fiber-laser-based distributed amplification, the lasing power distribution can be adjusted by tuning the reflectivity of the point-based mirrors located on the fiber span end [34] or by polarization control [47], making manipulation of the signal power distribution viable.

6. Discussion

The science and technology of long-cavity random DFB fiber lasers are both developing at a very fast rate since the concept was introduced in 2010 [25]. Despite rather nontrivial science underlying its operation, a random DFB fiber laser is not a complex and sophisticated engineering system—just the opposite. The combination of relative simplicity of implementation with very good laser performance is the key to the popularity of such devices and the growing number of applications.

The rich variety of demonstrated random fiber lasers is due to a combination of several factors: (a) the numbers of possible laser system configurations (tunable operation ([28,50]), filter-based configurations [49,51,64], half-open cavity setups [34,70], and others; (b) various gain mechanisms [73,90,95]; (c) varied output wavelengths [45,52,67,70,81,157]; (d) different operational regimes (CW, pulsating [106,107]), Q -switched random fiber lasers [158]; and (e) a range of fiber bases [37,45,68,103].

From a theoretical physics view point, random walk in 1D fiber is very different from that in 3D physical systems. In a 1D random walk (in an infinite system and given infinite time) the scattered wave (walker) will eventually return to the starting point. This is very distinct from 3D systems, making the corresponding 1D laser dissimilar to conventional 3D random lasers. The dynamics of light in a random medium, defined by multiple scattering of the photons on the fiber inhomogeneities, is strongly affected by the amplification due to SRS. In the context of Raman fiber lasers, spontaneous Raman scattering is analogous to fluorescence and SRS is similar to stimulated emission. The important difference, however, is the nonlinear nature of the Raman processes. The Raman gain is proportional to the intensity of the pump wave. This makes the spectral features of Raman fiber lasers nontrivial, as shown above in Section 3. Theoretical study of such lasers is far from over. We anticipate new interesting works at the interface of laser science and disordered theory.

As already mentioned, the relative simplicity of system configuration, the stability and flexibility of operating wavelengths and powers for the random fiber laser makes it attractive for various practical applications. For a single-sided grating-based laser, the lasing characteristics are determined primarily by the properties of the single FBG used at the edge, rather than the specifics of a fiber span section. Such a long distributed laser scheme overcomes the limitations imposed in many applications by fiber losses, and provides a higher SNR over longer spans of fiber, as compared to an external FBG interrogation. This higher sensitivity and point-selective response is very attractive for distributed sensing applications [147,148,150,151,159]. For example, a shift of the random lasing peak wavelength induced by the FBG strain at one end can be transduced as a power variation to be measured at the other free end of the laser [159]. Random lasing has also been used for pumping distributed amplifiers in BOTDA distributed sensing systems, extending the range of their operational distance to more than 100 kilometers [142,160,161]. The number of point-sensing FBGs could be increased, leading to multichannel sensor devices. This can be easily implemented by combining the concept of multiwavelength operation via a set of FBGs (see, for example, [55]) with sensing techniques [150] for simultaneous strain and temperature-independent sensing and multiple points. The spectral flatness of multiwavelength generation together with the possibility of fast switching between the wavelengths [64] offers promising opportunities for the multipoint distributed sensing using various random laser configurations that can be optimized and adjusted to specific applications.

Random distributed fiber laser amplification schemes have been deemed beneficial in long-haul fiber optic communication systems [69,142,143,162,163], as well as for fiber optic gyroscopes, with the promise of sensitivity improvement by a factor of 2 [164]. The functionalities of these systems can be extended further to time division multiplexed architectures, given the fact that, in comparison to linear or ring laser cavities, no distortion of the modulating frequency or self-mode-locking effects have been observed in these systems upon fast modulation of cavity losses [106,165]. Important applications of random fiber lasers can be found in imaging [15]. Conventional lasers provide good brightness; however, they are not suited for full-field imaging due to typical high spatial coherence that results in speckle and the corruption of images. Fiber random lasers can be an attractive solution providing low spatial coherence and high enough brightness.

Overall, the DFB random fiber laser is an interesting and growing area of science and technology at the interface of laser physics, the theory of disordered systems, optical engineering, fiber optics, theoretical physics, and various practical applications, and we anticipate new important developments in this field in the near future.

Acknowledgments

We would like to acknowledge financial support from the European Research Council (project UltraLaser), the FP7 Marie Curie IRSES (project Randfields), the Ministry of Education and Science of the Russian Federation (agreement No. 14.B25.31.0003), the Russian Foundation for Basic Research (grant 15-02-07925), a Presidential Grant for Young Researchers (grant 14.120.14.228-MK), the Dynasty Foundation, the Natural Science Foundation of China (61205048, 61290312), the Research Fund for the Doctoral Program of Higher Education of China (20120185120003), the Fundamental Research Funds for the Central Universities (ZYGX2012J002), the PCSIRT project (IRT1218), and the 111 project (B14039). S. A. B., E. V. P., and I. D. V. acknowledge financial support of their part of the work from the Russian Science Foundation (project no. 14-22-00118).

References

1. H. A. Macleod, *Thin-Film Optical Filters* (CRC Press, 2001).
2. P. Russell, "Photonic crystal fibers," *Science* **299**, 358–362 (2003).
3. T. Erdogan, "Fiber grating spectra," *J. Lightwave Technol.* **15**, 1277–1294 (1997).
4. R. Kashyap, *Fiber Bragg Gratings*, 2nd ed. (Academic, 2009).
5. S. Akiba, "Distributed feedback lasers," in *Encyclopedic Handbook of Integrated Optics*, K. Iga and Y. Kokubun, eds. (CRC Press, 2010), pp. 41–53.
6. J. Shi, S. ul Alam, and M. Ibsen, "Highly efficient Raman distributed feedback fibre lasers," *Opt. Express* **20**, 5082–5091 (2012).
7. L. E. Myers and W. R. Bosenberg, "Periodically poled lithium niobate and quasi-phase-matched optical parametric oscillators," *IEEE J. Quantum Electron.* **33**, 1663–1672 (1997).
8. S. A. Maier, *Plasmonics: Fundamentals and Applications* (Springer, 2007).
9. E. Le Ru and P. Etchegoin, *Principles of Surface-Enhanced Raman Spectroscopy: and Related Plasmonic Effects* (Elsevier, 2008).
10. D. R. Smith, J. B. Pendry, and M. C. Wiltshire, "Metamaterials and negative refractive index," *Science* **305**, 788–792 (2004).
11. F. Lederer, G. I. Stegeman, D. N. Christodoulides, G. Assanto, M. Segev, and Y. Silberberg, "Discrete solitons in optics," *Phys. Rep.* **463**, 1–126 (2008).
12. B. L. Ellerbroek, "First-order performance evaluation of adaptive-optics systems for atmospheric-turbulence compensation in extended-field-of-view astronomical telescopes," *J. Opt. Soc. Am. A* **11**, 783–805 (1994).
13. G. Keiser, *Optical Fiber Communications* (Wiley, 2003).
14. P. Vukusic and J. R. Sambles, "Photonic structures in biology," *Nature* **424**, 852–855 (2003).
15. B. Redding, S. F. Liew, R. Sarma, and H. Cao, "Compact spectrometer based on a disordered photonic chip," *Nat. Photonics* **7**, 746–751 (2013).

16. V. Y. F. Leung, A. Lagendijk, T. W. Tukker, A. P. Mosk, W. L. IJzerman, and W. L. Vos, "Interplay between multiple scattering, emission, and absorption of light in the phosphor of a white light-emitting diode," *Opt. Express* **22**, 8190–8204 (2014).
17. R. Ambartsumyan, N. Basov, P. Kryukov, and V. Letokhov, "A laser with a non-resonant feedback," *IEEE J. Quantum Electron.* **2**, 442–446 (1966).
18. N. M. Lawandy, R. Balachandran, A. Gomes, and E. Sauvain, "Laser action in strongly scattering media," *Nature* **368**, 436–438 (1994).
19. V. Markushev, N. É. Ter-Gabriélyan, C. M. Briskina, V. Belan, and V. Zolin, "Stimulated emission kinetics of neodymium powder lasers," *Sov. J. Quantum Electron.* **20**, 773–777 (1990).
20. H. Cao, Y. Zhao, S. Ho, E. Seelig, Q. Wang, and R. Chang, "Random laser action in semiconductor powder," *Phys. Rev. Lett.* **82**, 2278–2281 (1999).
21. Q. Song, S. Xiao, Z. Xu, J. Liu, X. Sun, V. Drachev, V. M. Shalaev, O. Akkus, and Y. L. Kim, "Random lasing in bone tissue," *Opt. Lett.* **35**, 1425–1427 (2010).
22. Q. Baudouin, N. Mercadier, V. Guarrera, W. Guerin, and R. Kaiser, "A cold-atom random laser," *Nat. Phys.* **9**, 357–360 (2013).
23. H. Cao, "Review on latest developments in random lasers with coherent feedback," *J. Phys.* **38**, 10497–10535 (2005).
24. H. Cao, "Lasing in random media," *Waves Random Media* **13**, R1–R39 (2003).
25. S. K. Turitsyn, S. A. Babin, A. E. El-Taher, P. Harper, D. V. Churkin, S. I. Kablukov, J. D. Ania-Castanon, V. Karalekas, and E. V. Podivilov, "Random distributed feedback fibre laser," *Nat. Photonics* **4**, 231–235 (2010).
26. S. K. Turitsyn, S. A. Babin, D. V. Churkin, I. D. Vatnik, M. Nikulin, and E. V. Podivilov, "Random distributed feedback fibre lasers," *Phys. Rep.* **542**, 133–193 (2014).
27. D. V. Churkin, S. A. Babin, A. E. El-Taher, P. Harper, S. I. Kablukov, V. Karalekas, J. D. Ania-Castanon, E. V. Podivilov, and S. K. Turitsyn, "Raman fiber lasers with a random distributed feedback based on Rayleigh scattering," *Phys. Rev. A* **82**, 033828 (2010).
28. S. A. Babin, A. E. El-Taher, P. Harper, E. V. Podivilov, and S. K. Turitsyn, "Tunable random fiber laser," *Phys. Rev. A* **84**, 021805 (2011).
29. I. D. Vatnik, D. V. Churkin, and S. A. Babin, "Power optimization of random distributed feedback fiber lasers," *Opt. Express* **20**, 28033 (2012).
30. Z. Wang, H. Wu, M. Fan, Y. Rao, I. Vatnik, E. Podivilov, S. Babin, D. Churkin, H. Zhang, P. Zhou, H. Xiao, and X. Wang, "Random fiber laser: simpler and brighter," *Opt. Photon. News* **25**(12), 30 (2014).
31. I. D. Vatnik, D. V. Churkin, E. V. Podivilov, and S. A. Babin, "High-efficiency generation in a short random fiber laser," *Laser Phys. Lett.* **11**, 075101 (2014).
32. H. Zhang, P. Zhou, H. Xiao, and X. Xu, "Efficient Raman fiber laser based on random Rayleigh distributed feedback with record high power," *Laser Phys. Lett.* **11**, 075104 (2014).
33. Z. Wang, H. Wu, M. Fan, L. Zhang, Y. Rao, W. Zhang, and X. Jia, "High power random fiber laser with short cavity length: theoretical and experimental investigations," *IEEE J. Sel. Top. Quantum Electron.* **21**, 0900506 (2015).
34. H. Wu, Z. Wang, M. Fan, L. Zhang, W. Zhang, and Y. Rao, "Role of the mirrors reflectivity in forward-pumped random fiber laser," *Opt. Express* **23**, 1421–1427 (2015).

35. S. Babin, I. Vatnik, A. Y. Laptev, M. Bubnov, and E. Dianov, "High-efficiency cascaded Raman fiber laser with random distributed feedback," *Opt. Express* **22**, 24929–24934 (2014).
36. M. Fan, Z. Wang, H. Wu, W. Sun, and L. Zhang, "Low-threshold, high-efficiency Random fiber laser with linear output," *IEEE Photon. Technol. Lett.* **27**, 319–322 (2015).
37. A. Lanin, D. Churkin, K. Golant, and S. Turitsyn, "Raman gain and random distributed feedback generation in nitrogen doped silica core fiber," in *Conference on Lasers and Electro-Optics Europe and International Quantum Electronics Conference (CLEO EUROPE/IQEC)* (IEEE, 2013).
38. S. A. Babin, E. I. Dontsova, and S. I. Kablukov, "Random fiber laser directly pumped by a high-power laser diode," *Opt. Lett.* **38**, 3301–3303 (2013).
39. S. I. Kablukov, E. I. Dontsova, E. A. Zlobina, I. N. Nemov, A. A. Vlasov, and S. A. Babin, "An LD-pumped Raman fiber laser operating below 1 μm ," *Laser Phys. Lett.* **10**, 085103 (2013).
40. T. Yao and J. Nilsson, "835 nm fiber Raman laser pulse pumped by a multimode laser diode at 806 nm," *J. Opt. Soc. Am. B* **31**, 882–888 (2014).
41. I. Vatnik, D. Churkin, E. Podivilov, and S. Babin, "High-efficiency generation in a short random fiber laser," *Laser Phys. Lett.* **11**, 075101 (2014).
42. A. R. Sarmani, M. H. Abu Bakar, A. A. A. Bakar, F. R. M. Adikan, and M. A. Mahdi, "Spectral variations of the output spectrum in a random distributed feedback Raman fiber laser," *Opt. Express* **19**, 14152–14159 (2011).
43. I. D. Vatnik, D. V. Churkin, and S. A. Babin, "Spectral width optimization in random DFB fiber laser," in *Conference on Lasers and Electro-Optics Europe and International Quantum Electronics Conference (CLEO EUROPE/IQEC)* (IEEE, 2013).
44. S. V. Smirnov and D. V. Churkin, "Modeling of spectral and statistical properties of a random distributed feedback fiber laser," *Opt. Express* **21**, 21236–21241 (2013).
45. I. D. Vatnik, D. V. Churkin, S. A. Babin, and S. K. Turitsyn, "Cascaded random distributed feedback Raman fiber laser operating at 1.2 μm ," *Opt. Express* **19**, 18486–18494 (2011).
46. D. V. Churkin, I. D. Vatnik, S. K. Turitsyn, and S. A. Babin, "Random distributed feedback Raman fiber laser operating in a 1.2 μm wavelength range," *Laser Phys.* **21**, 1525–1529 (2011).
47. H. Wu, Z. N. Wang, D. V. Churkin, I. D. Vatnik, M. Q. Fan, and Y. J. Rao, "Random distributed feedback Raman fiber laser with polarized pumping," *Laser Phys. Lett.* **12**, 015101 (2015).
48. D. V. Churkin, A. E. El-Taher, I. D. Vatnik, J. D. Ania-Castanon, P. Harper, E. V. Podivilov, S. A. Babin, and S. K. Turitsyn, "Experimental and theoretical study of longitudinal power distribution in a random DFB fiber laser," *Opt. Express* **20**, 11178–11188 (2012).
49. S. Sugavanam, N. Tarasov, X. Shu, and D. V. Churkin, "Narrow-band generation in random distributed feedback fiber laser," *Opt. Express* **21**, 16466–16472 (2013).
50. A. R. Sarmani, R. Zamiri, M. H. A. Bakar, B. Z. Azmi, A. W. Zaidan, and M. A. Mahdi, "Tunable Raman fiber laser induced by Rayleigh back-scattering in an ultra-long cavity," *J. Eur. Opt. Soc.* **6**, 11043 (2011).
51. Y. Y. Zhu, W. L. Zhang, and Y. Jiang, "Tunable multi-wavelength fiber laser based on random Rayleigh back-scattering," *IEEE Photon. Technol. Lett.* **25**, 1559–1561 (2013).

52. X. Du, H. Zhang, X. Wang, and P. Zhou, "Tunable random distributed feedback fiber laser operating at 1 μm ," *Appl. Opt.* **54**, 908–911 (2015).
53. S. A. Babin, D. V. Churkin, A. Ismagulov, S. Kablukov, E. Podivilov, M. Rybakov, and A. Vlasov, "All-fiber widely tunable Raman fiber laser with controlled output spectrum," *Opt. Express* **15**, 8438–8443 (2007).
54. K. Yeo, M. Mahdi, H. Mohamad, S. Hitam, and M. Mokhtar, "Widely tunable Raman ring laser using highly nonlinear fiber," *Laser Phys.* **19**, 2200–2203 (2009).
55. A. E. El-Taher, P. Harper, S. A. Babin, D. V. Churkin, E. V. Podivilov, J. D. Ania-Castanon, and S. K. Turitsyn, "Effect of Rayleigh-scattering distributed feedback on multiwavelength Raman fiber laser generation," *Opt. Lett.* **36**, 130–132 (2011).
56. A. El-Taher, M. Alcon-Camas, S. Babin, P. Harper, J. D. Ania-Castanón, and S. K. Turitsyn, "Dual-wavelength, ultralong Raman laser with Rayleigh-scattering feedback," *Opt. Lett.* **35**, 1100–1102 (2010).
57. A. Pinto, O. Frazão, J. Santos, and M. Lopez-Amo, "Multiwavelength fiber laser based on a photonic crystal fiber loop mirror with cooperative Rayleigh scattering," *Appl. Phys. B* **99**, 391–395 (2010).
58. A. Pinto, O. Frazão, J. Santos, and M. Lopez-Amo, "Multiwavelength Raman fiber lasers using Hi-Bi photonic crystal fiber loop mirrors combined with random cavities," *J. Lightwave Technol.* **29**, 1482–1488 (2011).
59. A. Pinto, M. Bravo, M. Fernandez-Vallejo, M. Lopez-Amo, J. Kobelke, and K. Schuster, "Suspended-core fiber Sagnac combined dual-random mirror Raman fiber laser," *Opt. Express* **19**, 11906–11915 (2011).
60. S. Sugavanam, Z. Yan, V. Kamynin, A. Kurkov, L. Zhang, and D. Churkin, "Multiwavelength generation in a random distributed feedback fiber laser using an all fiber Lyot filter," *Opt. Express* **22**, 2839–2844 (2014).
61. H. Tang, W. Zhang, Y. Rao, Y. Zhu, and Z. Wang, "Spectrum-adjustable random lasing in single-mode fiber controlled by a FBG," *Opt. Laser Technol.* **57**, 100–103 (2014).
62. M. Bravo Acha, V. DeMiguel-Soto, A. Ortigosa, and M. Lopez-Amo, "Fully switchable multi-wavelength fiber laser based interrogator system for remote and versatile fiber optic sensors multiplexing structures," *Proc. SPIE* **9157**, 91576P (2014).
63. Y. Zhu, W. Zhang, and Y. Jiang, "Tunable multi-wavelength fiber laser based on random Rayleigh back-scattering," *IEEE Photon. Technol. Lett.* **25**, 1559–1561 (2013).
64. V. DeMiguel-Soto, M. Bravo, and M. Lopez-Amo, "Fully switchable multiwavelength fiber laser assisted by a random mirror," *Opt. Lett.* **39**, 2020–2023 (2014).
65. L. Chen and Y. Ding, "Random distributed feedback fiber laser pumped by an ytterbium doped fiber laser," *Optik* **125**, 3663–3665 (2014).
66. H. Zhang, H. Xiao, P. Zhou, X. Wang, and X. Xu, "High-power random distributed feedback Raman fiber laser operating at 1.2- μm ," *Chin. Opt. Lett.* **12**, 073501 (2014).
67. W. L. Zhang, Y. J. Rao, J. M. Zhu, Z. X. Y. Wang, Z. Nan, and X. H. Jia, "Low threshold 2nd-order random lasing of a fiber laser with a half-opened cavity," *Opt. Express* **20**, 14400–14405 (2012).
68. W. L. Zhang, Y. Y. Zhu, Y. J. Rao, Z. N. Wang, X. H. Jia, and H. Wu, "Random fiber laser formed by mixing dispersion compensated fiber and single mode fiber," *Opt. Express* **21**, 8544–8549 (2013).

69. X.-H. Jia, Y.-J. Rao, C.-X. Yuan, J. Li, X.-D. Yan, Z.-N. Wang, W.-L. Zhang, H. Wu, Y.-Y. Zhu, and F. Peng, "Hybrid distributed Raman amplification combining random fiber laser based 2nd-order and low-noise LD based 1st-order pumping," *Opt. Express* **21**, 24611–24619 (2013).
70. Z. Wang, H. Wu, M. Fan, Y. Rao, X. Jia, and W. Zhang, "Third-order random lasing via Raman gain and Rayleigh feedback within a half-open cavity," *Opt. Express* **21**, 20090–20095 (2013).
71. S. A. Babin, E. I. Dontsova, I. D. Vatnik, and S. I. Kablukov, "Second harmonic generation of a random fiber laser with Raman gain," *Proc. SPIE* **9347**, 934710 (2015).
72. M. Pang, X. Bao, and L. Chen, "Observation of narrow linewidth spikes in the coherent Brillouin random fiber laser," *Opt. Lett.* **38**, 1866–1868 (2013).
73. M. Pang, X. Bao, L. Chen, Z. Qin, Y. Lu, and P. Lu, "Frequency stabilized coherent Brillouin random fiber laser: theory and experiments," *Opt. Express* **21**, 27155–27168 (2013).
74. M. Pang, S. Xie, X. Bao, D.-P. Zhou, Y. Lu, and L. Chen, "Rayleigh scattering-assisted narrow linewidth Brillouin lasing in cascaded fiber," *Opt. Lett.* **37**, 3129–3131 (2012).
75. A. A. Fotiadi and R. V. Kiyan, "Cooperative stimulated Brillouin and Rayleigh backscattering process in optical fiber," *Opt. Lett.* **23**, 1805–1807 (1998).
76. B. Saxena, Z. Ou, X. Bao, and L. Chen, "Low frequency-noise random fiber laser with bi-directional SBS and Rayleigh feedback," *IEEE Photon. Technol. Lett.* **27**, 490–493 (2015).
77. B. Min, P. Kim, and N. Park, "Flat amplitude equal spacing 798-channel Rayleigh-assisted Brillouin/Raman multiwavelength comb generation in dispersion compensating fiber," *IEEE Photon. Technol. Lett.* **13**, 1352–1354 (2001).
78. K.-D. Park, B. Min, P. Kim, N. Park, J.-H. Lee, and J.-S. Chang, "Dynamics of cascaded Brillouin-Rayleigh scattering in a distributed fiber Raman amplifier," *Opt. Lett.* **27**, 155–157 (2002).
79. A. Zamzuri, M. Md Ali, A. Ahmad, R. Mohamad, and M. Mahdi, "Brillouin-Raman comb fiber laser with cooperative Rayleigh scattering in a linear cavity," *Opt. Lett.* **31**, 918–920 (2006).
80. H. Martins, M. B. Marques, and O. Frazão, "Comparison of Brillouin-Raman comb fiber laser in two different configurations," *Laser Phys.* **21**, 1925–1931 (2011).
81. R. Teng, Y. Ding, and L. Chen, "Random fiber laser operating at 1,115 nm," *Appl. Phys. B* **111**, 169–172 (2013).
82. R. S. Shargh, M. H. Al-Mansoori, S. B. A. Anas, R. K. Z. Sahbudin, and M. A. Mahdi, "OSNR enhancement utilizing large effective area fiber in a multiwavelength Brillouin-Raman fiber laser," *Laser Phys. Lett.* **8**, 139–143 (2011).
83. R. S. Shargh, M. Al-Mansoori, S. Anas, R. Sahbudin, A. Zamzuri, and M. Mahdi, "Improvement of comb lines quality employing double-pass architecture in Brillouin-Raman laser," *Laser Phys. Lett.* **8**, 823–827 (2011).
84. Z. Wang, H. Wu, M. Fan, Y. Li, Y. Gong, and Y. Rao, "Broadband flat-amplitude multiwavelength Brillouin-Raman fiber laser with spectral reshaping by Rayleigh scattering," *Opt. Express* **21**, 29358–29363 (2013).
85. H. Wu, Z. Wang, X. Jia, P. Li, M. Fan, Y. Li, and Y. Zhu, "Flat amplitude multiwavelength Brillouin Raman random fiber laser with a half-open cavity," *Appl. Phys. B* **112**, 467–471 (2013).

86. H. Ahmad, M. Zulkifli, M. Jemangin, and S. Harun, "Distributed feedback multimode Brillouin-Raman random fiber laser in the S-band," *Laser Phys. Lett.* **10**, 055102 (2013).
87. T. Zhu, X. Bao, and L. Chen, "A self-gain random distributed feedback fiber laser based on stimulated Rayleigh scattering," *Opt. Commun.* **285**, 1371–1374 (2012).
88. T. Zhu, X. Bao, L. Chen, H. Liang, and Y. Dong, "Experimental study on stimulated Rayleigh scattering in optical fibers," *Opt. Express* **18**, 22958–22963 (2010).
89. M. Abu Bakar, F. M. Adikan, and M. Mahdi, "Rayleigh-based Raman fiber laser with passive erbium-doped fiber for secondary pumping effect in remote L-band erbium-doped fiber amplifier," *IEEE Photon. J.* **4**, 1042–1050 (2012).
90. P. Zhang, T. Wang, Q. Jia, X. Liu, M. Kong, S. Tong, and H. Jiang, "A novel fiber laser based on Rayleigh scattering feedback with a half-opened cavity," *Proc. SPIE* **906**, 890617 (2013).
91. L. Wang, X. Dong, P. P. Shum, C. Huang, and H. Su, "Erbium-doped fiber laser with distributed Rayleigh output mirror," *Laser Phys.* **24**, 115101 (2014).
92. W. L. Zhang, S. W. Li, R. Ma, Y. J. Rao, Y. Y. Zhu, Z. N. Wang, X. H. Jia, and J. Li, "Random distributed feedback fiber laser based on combination of Er-doped fiber and single-mode Fiber," *IEEE J. Sel. Top. Quantum Electron.* **21**, 44–49 (2015).
93. C. Huang, X. Dong, N. Zhang, S. Zhang, and P. P. Shum, "Multiwavelength Brillouin-erbium random fiber laser incorporating a chirped fiber Bragg grating," *IEEE J. Sel. Top. Quantum Electron.* **20**, 902405 (2014).
94. G. Mamdoohi, A. R. Sarmani, A. F. Abas, M. H. Yaacob, M. Mokhtar, and M. A. Mahdi, "20 GHz spacing multi-wavelength generation of Brillouin-Raman fiber laser in a hybrid linear cavity," *Opt. Express* **21**, 18724–18732 (2013).
95. C. Huang, X. Dong, S. Zhang, N. Zhang, and P. Shum, "Cascaded random fiber laser based on hybrid Brillouin-erbium fiber gains," *IEEE Photon. Technol. Lett.* **26**, 1287–1290 (2014).
96. A. Al-Alimi, M. Yaacob, and A. Abas, "Half-linear cavity multiwavelength Brillouin-erbium fiber laser," *J. Eur. Opt. Soc. Rapid Pub.* **9**, 14051 (2014).
97. O. Shapira and B. Fischer, "Localization of light in a random-grating array in a single-mode fiber," *J. Opt. Soc. Am. B* **22**, 2542–2552 (2005).
98. Y. Bliokh, E. I. Chaikina, N. Lizárraga, E. R. Méndez, V. Freilikher, and F. Nori, "Disorder-induced cavities, resonances, and lasing in randomly layered media," *Phys. Rev. B* **86**, 054204 (2012).
99. M. Gagné and R. Kashyap, "Random fiber Bragg grating Raman fiber laser," *Opt. Lett.* **39**, 2755–2758 (2014).
100. S. Derevyanko, "Design of a flat-top fiber Bragg filter via quasi-random modulation of the refractive index," *Opt. Lett.* **33**, 2404–2406 (2008).
101. C. J. S. de Matos, L. D. S. Menezes, A. M. Brito-Silva, M. A. M. Gámez, A. S. L. Gomes, and C. B. de Araújo, "Random fiber laser," *Phys. Rev. Lett.* **99**, 153903 (2007).
102. Z. Hu, Q. Zhang, B. Miao, Q. Fu, G. Zou, Y. Chen, Y. Luo, D. Zhang, P. Wang, H. Ming, and Q. Zhang, "Coherent random fiber laser based on nanoparticles scattering in the extremely weakly scattering regime," *Phys. Rev. Lett.* **109**, 253901 (2012).

103. Z. Hu, B. Miao, T. Wang, Q. Fu, D. Zhang, H. Ming, and Q. Zhang, "Disordered microstructure polymer optical fiber for stabilized coherent random fiber laser," *Opt. Lett.* **38**, 4644–4647 (2013).
104. Z. Hu, P. Gao, K. Xie, Y. Liang, and H. Jiang, "Wavelength control of random polymer fiber laser based on adaptive disorder," *Opt. Lett.* **39**, 6911–6914 (2014).
105. Z. Hu, Y. Liang, K. Xie, P. Gao, D. Zhang, H. Jiang, F. Shi, L. Yin, J. Gao, H. Ming, and Q. Zhang, "Gold nanoparticle-based plasmonic random fiber laser," *J. Opt.* **17**, 035001 (2015).
106. M. Bravo, M. Fernandez-Vallejo, and M. Lopez-Amo, "Internal modulation of a random fiber laser," *Opt. Lett.* **38**, 1542–1544 (2013).
107. H. Zhang, H. Xiao, P. Zhou, X. Wang, and X. Xu, "Random distributed feedback Raman fiber laser with short cavity and its temporal properties," *IEEE Photon. Technol. Lett.* **26**, 1605–1608 (2014).
108. A. Lanin, S. Sergeev, D. Nasiev, D. Churkin, and S. Turitsyn, "On-off and multistate intermittencies in cascaded random distributed feedback fibre laser," in *Conference on Lasers and Electro-Optics Europe and International Quantum Electronics Conference (CLEO EUROPE/IQEC)* (IEEE, 2013).
109. G. Ravet, A. Fotiadi, M. Blondel, and P. Mégret, "Passive Q-switching in all-fibre Raman laser with distributed Rayleigh feedback," *Electron. Lett.* **40**, 528–529 (2004).
110. A. A. Fotiadi, P. Mégret, and M. Blondel, "Dynamics of a self-Q-switched fiber laser with a Rayleigh-stimulated Brillouin scattering ring mirror," *Opt. Lett.* **29**, 1078–1080 (2004).
111. S. Chernikov, Y. Zhu, J. Taylor, and V. Gapontsev, "Supercontinuum self-Q-switched ytterbium fiber laser," *Opt. Lett.* **22**, 298–300 (1997).
112. Y. Tang, X. Li, and Q. J. Wang, "High-power passively Q-switched thulium fiber laser with distributed stimulated Brillouin scattering," *Opt. Lett.* **38**, 5474–5477 (2013).
113. O. Gorbunov, S. Sugavanam, and D. Churkin, "Intensity dynamics and statistical properties of random distributed feedback fiber laser," *Opt. Lett.* **40**, 1783–1786 (2015).
114. E. G. Turitsyna, S. V. Smirnov, S. Sugavanam, N. Tarasov, X. Shu, S. A. Babin, E. V. Podivilov, D. V. Churkin, G. Falkovich, and S. K. Turitsyn, "The laminar-turbulent transition in a fibre laser," *Nat. Photonics* **7**, 783–786 (2013).
115. A. Picozzi, J. Garnier, T. Hansson, P. Suret, S. Randoux, G. Millot, and D. Christodoulides, "Optical wave turbulence: towards a unified nonequilibrium thermodynamic formulation of statistical nonlinear optics," *Phys. Rep.* **542**, 1–132 (2014).
116. M. Conforti, A. Mussot, J. Fatome, A. Picozzi, S. Pitois, C. Finot, M. Haelterman, B. Kibler, C. Michel, and G. Millot, "Turbulent dynamics of an incoherently pumped passive optical fiber cavity: quasi-solitons, dispersive waves, and extreme events," *Phys. Rev. A* **91**, 023823 (2015).
117. D. Solli, C. Ropers, P. Koonath, and B. Jalali, "Optical rogue waves," *Nature* **450**, 1054–1057 (2007).
118. D. V. Churkin, O. A. Gorbunov, and S. V. Smirnov, "Extreme value statistics in Raman fiber lasers," *Opt. Lett.* **36**, 3617–3619 (2011).
119. S. Randoux and P. Suret, "Experimental evidence of extreme value statistics in Raman fiber lasers," *Opt. Lett.* **37**, 500–502 (2012).

120. C. Lecaplain, P. Grelu, J. Soto-Crespo, and N. Akhmediev, "Dissipative rogue waves generated by chaotic pulse bunching in a mode-locked laser," *Phys. Rev. Lett.* **108**, 233901 (2012).
121. K. Hammani, A. Picozzi, and C. Finot, "Extreme statistics in Raman fiber amplifiers: from analytical description to experiments," *Opt. Commun.* **284**, 2594–2603 (2011).
122. N. Akhmediev, J. Dudley, D. Solli, and S. Turitsyn, "Recent progress in investigating optical rogue waves," *J. Opt.* **15**, 060201 (2013).
123. M. Onorato, S. Residori, U. Bortolozzo, A. Montina, and F. Arecchi, "Rogue waves and their generating mechanisms in different physical contexts," *Phys. Rep.* **528**, 47–89 (2013).
124. J. M. Dudley, F. Dias, M. Erkintalo, and G. Genty, "Instabilities, breathers and rogue waves in optics," *Nat. Photonics* **8**, 755–764 (2014).
125. D. V. Churkin, S. V. Smirnov, and E. V. Podivilov, "Statistical properties of partially coherent CW fiber lasers," *Opt. Lett.* **35**, 3288–3290 (2010).
126. S. Randoux, N. Dalloz, and P. Suret, "Intracavity changes in the field statistics of Raman fiber lasers," *Opt. Lett.* **36**, 790–792 (2011).
127. D. V. Churkin and S. V. Smirnov, "Numerical modelling of spectral, temporal and statistical properties of Raman fiber lasers," *Opt. Commun.* **285**, 2154–2160 (2012).
128. A. E. Bednyakova, O. A. Gorbunov, M. O. Politko, S. I. Kablukov, S. V. Smirnov, D. V. Churkin, M. P. Fedoruk, and S. A. Babin, "Generation dynamics of the narrowband Yb-doped fiber laser," *Opt. Express* **21**, 8177–8182 (2013).
129. S. Randoux, P. Walczak, M. Onorato, and P. Suret, "Intermittency in integrable turbulence," *Phys. Rev. Lett.* **113**, 113902 (2014).
130. O. Gorbunov, S. Sugavanam, and D. Churkin, "Revealing statistical properties of quasi-CW fibre lasers in bandwidth-limited measurements," *Opt. Express* **22**, 28071–28076 (2014).
131. S. K. Turitsyn, A. E. Bednyakova, M. P. Fedoruk, A. I. Latkin, A. A. Fotiadi, A. S. Kurkov, and E. Sholokhov, "Modeling of CW Yb-doped fiber lasers with highly nonlinear cavity dynamics," *Opt. Express* **19**, 8394–8405 (2011).
132. S. A. Babin, D. V. Churkin, A. E. Ismagulov, S. I. Kablukov, and E. V. Podivilov, "Four-wave-mixing-induced turbulent spectral broadening in a long Raman fiber laser," *J. Opt. Soc. Am. B* **24**, 1729–1738 (2007).
133. S. A. Babin, D. V. Churkin, A. E. Ismagulov, S. I. Kablukov, and E. V. Podivilov, "Spectral broadening in Raman fiber lasers," *Opt. Lett.* **31**, 3007–3009 (2006).
134. S. A. Babin, D. V. Churkin, A. E. Ismagulov, S. I. Kablukov, and E. V. Podivilov, "Turbulence-induced square-root broadening of the Raman fiber laser output spectrum," *Opt. Lett.* **33**, 633–635 (2008).
135. I. D. Vatnik and D. V. Churkin, "Modeling of the spectrum in a random distributed feedback fiber laser within the power balance modes," *Proc. SPIE* **9135**, 91351Z (2014).
136. C. R. Giles and E. Desurvire, "Modeling erbium-doped fiber amplifiers," *J. Lightwave Technol.* **9**, 271–283 (1991).
137. A. L. Schawlow and C. H. Townes, "Infrared and optical masers," *Phys. Rev.* **112**, 1940–1949 (1958).

138. D. V. Churkin, I. V. Kolokolov, E. V. Podivilov, I. D. Vatnik, M. A. Nikulin, S. S. Vergeles, I. S. Terekhov, V. V. Lebedev, G. Falkovich, S. A. Babin, and S. K. Turitsyn, “Wave kinetics of random fibre lasers,” *Nat. Commun.* **2**, 6214 (2015).
139. V. E. Zakharov, V. S. L’Vov, and G. Falkovich, *Kolmogorov Spectra of Turbulence I. Wave Turbulence* (Springer, 1992).
140. S. Nazarenko, *Wave Turbulence*, Vol. **825** of Lecture Notes in Physics (Springer, 2011).
141. I. Kolokolov, V. Lebedev, E. Podivilov, and S. Vergeles, “Theory of a random fiber laser,” *J. Exp. Theor. Phys.* **119**, 1134–1139 (2014).
142. X.-H. Jia, Y.-J. Rao, F. Peng, Z.-N. Wang, W.-L. Zhang, H.-J. Wu, and Y. Jiang, “Random-lasing-based distributed fiber-optic amplification,” *Opt. Express* **21**, 6572–6577 (2013).
143. J. Nuño, M. Alcon-Camas, and J. D. Ania-Castañón, “RIN transfer in random distributed feedback fiber lasers,” *Opt. Express* **20**, 27376–27381 (2012).
144. S. Babin, D. Churkin, A. Fotiadi, S. Kablukov, O. Medvedkov, and E. Podivilov, “Relative intensity noise in cascaded-Raman fiber lasers,” *IEEE Photon. Technol. Lett.* **17**, 2553–2555 (2005).
145. B. Saxena, X. Bao, and L. Chen, “Suppression of thermal frequency noise in erbium-doped fiber random lasers,” *Opt. Lett.* **39**, 1038–1041 (2014).
146. Y. Li, P. Lu, X. Bao, and Z. Ou, “Random spaced index modulation for a narrow linewidth tunable fiber laser with low intensity noise,” *Opt. Lett.* **39**, 2294–2297 (2014).
147. Z. N. Wang, Y. J. Rao, H. Wu, P. Y. Li, Y. Jiang, X. H. Jia, and W. L. Zhang, “Long-distance fiber-optic point-sensing systems based on random fiber lasers,” *Opt. Express* **20**, 17695–17700 (2012).
148. M. Fernandez-Vallejo, M. Bravo, and M. Lopez-Amo, “Ultra-long laser systems for remote fiber Bragg gratings arrays interrogation,” *IEEE Photon. Technol. Lett.* **25**, 1362–1364 (2013).
149. A. M. R. Pinto, M. Lopez-Amo, J. Kobelke, and K. Schuster, “Temperature fiber laser sensor based on a hybrid cavity and a random mirror,” *J. Lightwave Technol.* **30**, 1168–1172 (2012).
150. H. F. Martins, M. B. Marques, and O. Frazão, “Temperature-insensitive strain sensor based on four-wave mixing using Raman fiber Bragg grating laser sensor with cooperative Rayleigh scattering,” *Appl. Phys. B* **104**, 957–960 (2011).
151. H. Martins, M. B. Marques, and O. Frazão, “300 km-ultralong Raman fiber lasers using a distributed mirror for sensing applications,” *Opt. Express* **19**, 18149–18154 (2011).
152. S. K. Turitsyn, J. D. Ania-Castañón, S. A. Babin, V. Karalekas, P. Harper, D. Churkin, S. I. Kablukov, A. E. El-Taher, E. V. Podivilov, and V. K. Mezentsev, “270-km ultralong Raman fiber laser,” *Phys. Rev. Lett.* **103**, 133901 (2009).
153. T. Saitoh, K. Nakamura, Y. Takahashi, H. Iida, Y. Iki, and K. Miyagi, “Ultra-long-distance (230 km) FBG sensor system,” *Proc. SPIE* **7004**, 70046C (2008).
154. X.-H. Jia, Y.-J. Rao, Z.-N. Wang, W.-L. Zhang, Y. Jiang, J.-M. Zhu, and Z.-X. Yang, “Towards fully distributed amplification and high-performance long-range distributed sensing based on random fiber laser,” *Proc. SPIE* **8421**, 842127 (2012).

155. X.-H. Jia, Y.-J. Rao, Z.-N. Wang, W.-L. Zhang, C.-X. Yuan, X.-D. Yan, J. Li, H. Wu, Y.-Y. Zhu, and F. Peng, "Distributed Raman amplification using ultra-long fiber laser with a ring cavity: characteristics and sensing application," *Opt. Express* **21**, 21208–21217 (2013).
156. Z. N. Wang, J. J. Zeng, J. Li, M. Q. Fan, H. Wu, F. Peng, L. Zhang, Y. Zhou, and Y. J. Rao, "Ultra-long phase-sensitive OTDR with hybrid distributed amplification," *Opt. Lett.* **39**, 5866–5869 (2014).
157. S. A. Babin, E. I. Dontsova, and S. I. Kablukov, "980-nm random fiber laser directly pumped by a high-power 938-nm laser diode," *Proc. SPIE* **8961**, 89612F (2014).
158. Y. Tang and J. Xu, "A random Q-switched fiber laser," *Sci. Rep.* **5**, 9338 (2015).
159. H. Martins, M. Marques, and O. Frazão, "Intensity vibration sensor based on Raman fiber laser using a distributed mirror combined with Bragg grating structures," *Appl. Phys. B* **114**, 455–459 (2014).
160. J. Nuño and J. D. Ania-Castañón, "Cavity and random ultralong fibre laser amplification in BOTDAs: a comparison," *Laser Phys.* **24**, 065107 (2014).
161. Y.-J. Rao, X.-H. Jia, Z.-N. Wang, W.-L. Zhang, C.-X. Yuan, J. Li, X.-D. Yan, H. Wu, Y.-Y. Zhu, and F. Peng, "154.4 km BOTDA based on hybrid distributed Raman amplifications," *Proc. SPIE* **9157**, 91575P (2014).
162. P. Rosa, M. Tan, S. Le, I. Phillips, J. D. Ania-Castanon, S. Sygletos, and P. Harper, "Unrepeated DP-QPSK transmission over 352.8 km SMF using random DFB fibre laser amplification," *IEEE Photon. Technol. Lett.* **27**, 1189–1192 (2015).
163. M. Tan, P. Rosa, I. Phillips, and P. Harper, "Extended reach of 116 Gb/s DP-QPSK transmission using random DFB fiber laser based Raman amplification and bidirectional second-order pumping," in *Optical Fiber Communication Conference* (Optical Society of America, 2015), paper W4E.
164. J. Nuño and J. D. Ania-Castañón, "Fiber Sagnac interferometers with ultralong and random distributed feedback Raman laser amplification," *Opt. Lasers Eng.* **54**, 21–26 (2014).
165. M. Fernandez-Vallejo, S. Rota-Rodrigo, and M. Lopez-Amo, "Comparative study of ring and random cavities for fiber lasers," *Appl. Opt.* **53**, 3501–3507 (2014).